frontiers | Frontiers in Physics

TYPE Original Research
PUBLISHED 04 January 2023
DOI 10.3389/fphy.2022.1086809

OPEN ACCESS

EDITED BY
Leonardo Makinistian,
Instituto de Física Aplicada (UNSL-CONICET), Argentina

REVIEWED BY
Lucián Zastko,
Cancer Research Institute (SAS), Slovakia
Priyanka Shaw,
University of Antwerp, Belgium

*CORRESPONDENCE
Wendy S. Beane,
wendy.beane@wmich.edu

SPECIALTY SECTION
This article was submitted to Biophysics, a section of the journal Frontiers in Physics

RECEIVED 01 November 2022
ACCEPTED 15 December 2022
PUBLISHED 04 January 2023

CITATION
Kinsey LJ, Van Huizen AV and Beane WS (2023), Weak magnetic fields modulate superoxide to control planarian regeneration.
Front. Phys. 10:1086809.
doi: 10.3389/fphy.2022.1086809

Weak magnetic fields modulate superoxide to control planarian regeneration

Luke J. Kinsey[1], Alanna V. Van Huizen[1,2] and Wendy S. Beane[1]*

[1]Department of Biological Sciences, Western Michigan University, Kalamazoo, MI, United States, [2]Department of Hematology, St. Jude Children's Research Hospital, Memphis, TN, United States

Reactive oxygen species (ROS) signaling regulates cell behaviors and tissue growth in development, regeneration, and cancer. Commonly, ROS are modulated pharmacologically, which while effective comes with potential complications such as off-target effects and lack of drug tolerance. Thus, additional non-invasive therapeutic methods are necessary. Recent advances have highlighted the use of weak magnetic fields (WMFs, <1 mT) as one promising approach. We previously showed that 200 μT WMFs inhibit ROS formation and block planarian regeneration. However, WMF research in different model systems at various field strengths have produced a range of results that do not fit common dose response curves, making it unclear if WMF effects are predictable. Here, we test hypotheses based on spin state theory and the radical pair mechanism, which outlines how magnetic fields can alter the formation of radical pairs by changing electron spin states. This mechanism suggests that across a broad range of field strengths (0–900 μT) some WMF exposures should be able to inhibit while others promote ROS formation in a binary fashion. Our data reveal that WMFs can be used for directed manipulation of stem cell proliferation, differentiation, and tissue growth in predictable ways for both loss and gain of function during regenerative growth. Furthermore, we examine two of the most common ROS signaling effectors, hydrogen peroxide and superoxide, to begin the identification and elucidation of the specific molecular targets by which WMFs affect tissue growth. Together, our data reveal that the cellular effects of WMF exposure are highly dependent on ROS, and we identify superoxide as a specific ROS being modulated. Altogether, these data highlight the possibilities of using WMF exposures to control ROS signaling *in vivo* and represent an exciting new area of research.

KEYWORDS

planaria, ROS signaling, regeneration, stem cells, quantum biology, static weak magnetic fields, radical pair mechanism, reactive oxygen species

Introduction

Reactive oxygen species (ROS) are a group of oxygen-containing molecules with varying reactivity. Intracellular ROS are typically derived from molecular oxygen (O_2) and include hydrogen peroxide (H_2O_2), the superoxide anion (O_2^-), and the hydroxyl radical ($^{\bullet}OH$), species which are known to participate in cellular reactions and initiate ROS-

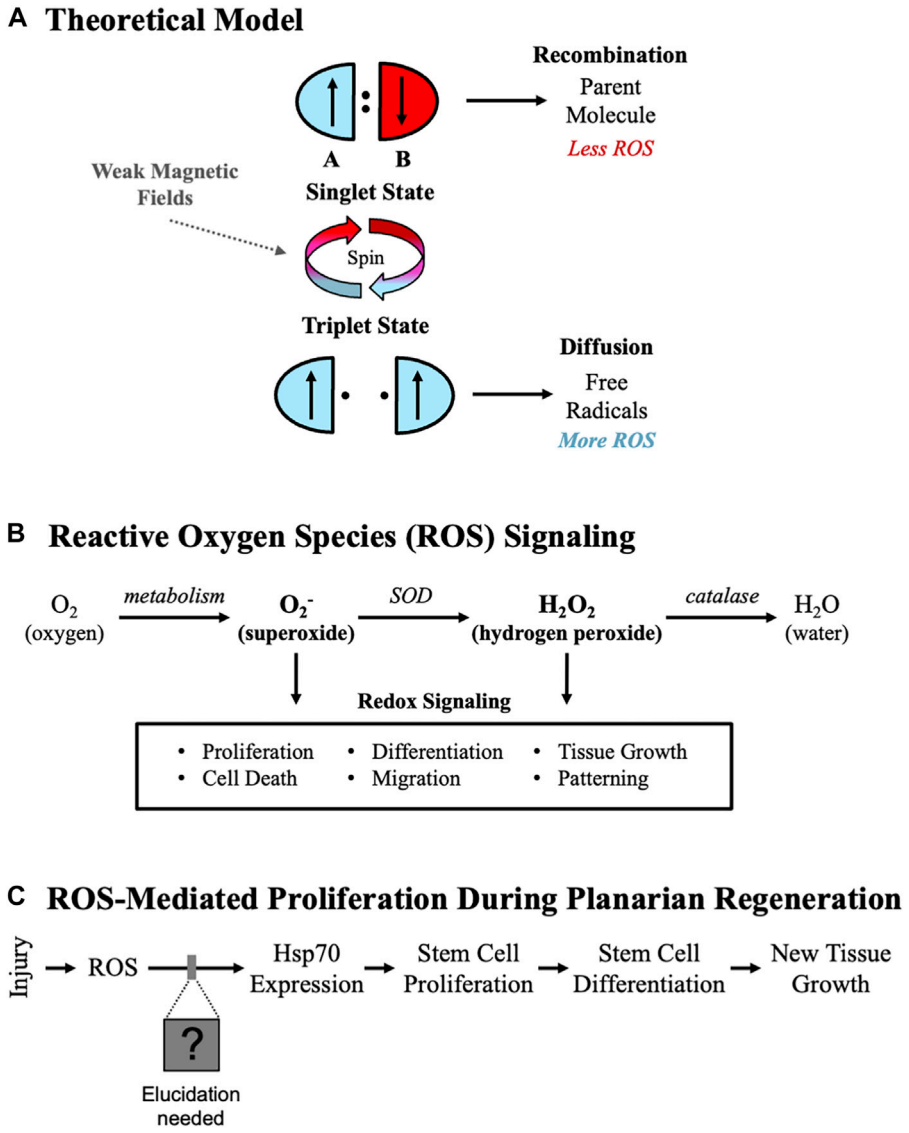

FIGURE 1
Controlling Stem Cell-Mediated Tissue Growth. **(A)** Theoretical model. Weak magnetic fields alter electron spins (represented by up or down arrows) *via* the radical pair mechanism, changing reactive oxygen species (ROS) levels. The antiparallel valence spins of the singlet state promote recombination, resulting in less ROS. The parallel spins of the triplet state drive diffusion, increasing ROS. **(B)** ROS signaling pathways. Consensus pathway from the literature for ROS signaling starting with molecular oxygen. Two of the main species known to affect cellular activities are superoxide ($O2^{-}$) and hydrogen peroxide (H_2O_2). (SOD = superoxide dismutase). **(C)** ROS-mediated proliferation in planarians. Experimentally derived ROS-mediated events during planarian regeneration, where changes in ROS levels affect Heat Shock Protein 70 (Hsp70), which is required for stem cell-mediated tissue growth after injury.

mediated signaling [1]. The mechanics of ROS signaling are complex and based on threshold levels in a context-dependent fashion. For example, low levels of ROS are required for cellular metabolism and homeostasis. In contrast, exceedingly high ROS levels lead to oxidative stress, and thus nonspecific damage to a cell's DNA, protein, and lipid structures [2, 3]. Threshold increases in ROS can cause imbalances in a cell's redox state, which can even lead to disease states such as cancer and aging [4]. However, within certain physiological parameters (that are not fully understood), moderate increases in ROS function to modulate traditional cell signaling pathways (termed redox signaling) [5, 6]. In this way, ROS signaling regulates many important cellular processes, including cell migration, proliferation, apoptosis, and differentiation [7–9].

Recent findings, including our own, demonstrate that ROS signaling is also critical for driving stem cell-mediated tissue

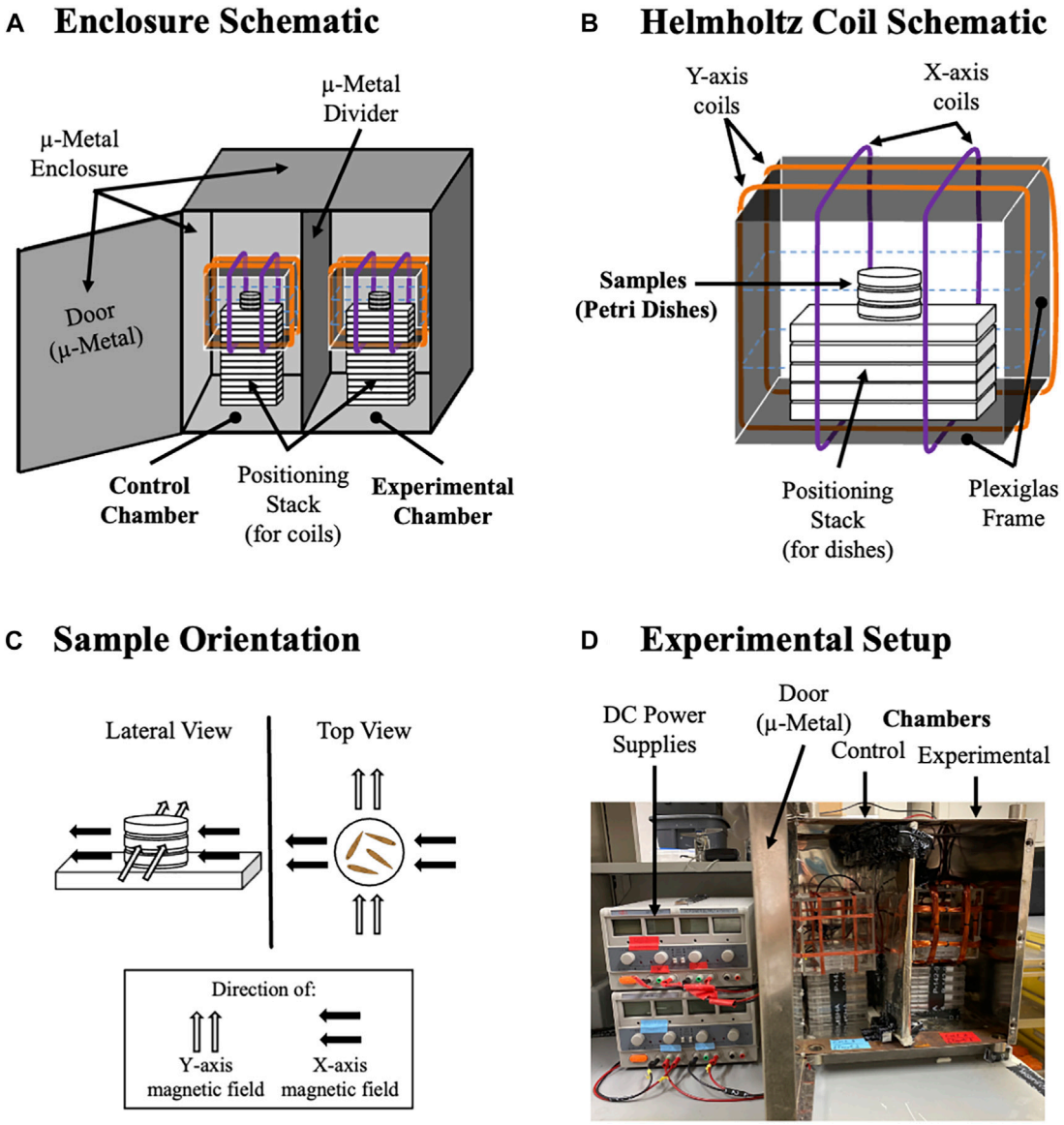

FIGURE 2
Setup for Environmentally-Controlled Magnetic Field Exposure. **(A)** Diagram of MagShield Box with Coils. The μ-metal enclosure has two chambers separated by a μ-metal partition. Coils are stacked on empty, 24-well culture plates (plastic) to position them in the center of each chamber. Left side is the control chamber (set at 45 μT), and right side is the experimental chamber. **(B)** Diagram of Helmholtz Coils. Inside the square plexiglass frame, three 35 mm Petri dishes hold samples (worms), with additional empty 24-well culture plates used to position Petri dishes in the center of each coil. Orange lines are *Y*-axis coils. Purple lines are *X*-axis coils. (Blue dotted lines are *Z*-axis coils, which were not used in this study). **(C)** Location of Petri Dishes in the Uniform Magnetic Fields Produced. Black arrows show the direction of the *X*-axis magnetic field. Gray arrows show the *Y*-axis field direction. **(D)** Experimental Setup. DC power supplies are positioned to the left of the MagShield Box, shown with door open (door is kept shut during experiments).

growth [10–15]. ROS signaling plays a role in cardiomyocyte differentiation, promotes transient stem cell proliferation in mouse skin, and is required for regenerative outgrowth in a myriad of animal model systems [14–17]. Maintenance of stem cell populations requires careful control of ROS levels, which can direct them to remain quiescent, proliferate, or differentiate depending on concentration [18]. ROS signaling plays an equally complex role during tumorigenesis. The upregulation of ROS scavengers (antioxidants) is a hallmark of many cancers, functioning to allow tumorigenic cells to bypass apoptosis; however, tumor progression can be later promoted by increased ROS levels, and ROS scavenging has been found to prevent the development and progression of many cancers in cell culture [19–21].

The data highlight the importance of ROS manipulation as a therapeutic target in interventions where tight control of proliferating cells and tissue growth (such as in regenerative medicine and cancer treatments) is required [22]. Currently, many of the standard molecular-genetic (pharmacological) approaches to manipulating ROS come with potential therapeutic complications such as drug toxicity. To bypass these issues, research has turned to the use of nanoparticles for targeted delivery; but these efforts have been hampered in part due to patient heterogeneity that interferes with successful distribution and/or function [23, 24]. Thus, the identification of additional methods to alter ROS levels is warranted for improved care and experimental approaches alike. Recent advances in our understanding of how biological systems interact with electromagnetic radiation suggest there is potential for finding such new approaches to manipulating ROS *in vivo* by using weak magnetic fields (WMFs, <1 mT), a form of non-ionizing radiation.

A predominant theory for understanding the biological effects of WMF exposures centers on the radical pair mechanism, which has been reviewed in detail [25–30]. Briefly, theoretical modeling (Figure 1A) suggests that WMFs can modulate radical pairs through changes in the angular momentum of lone electrons (spin state theory). Parent molecules can both dissociate into radical pairs and recombine at given rates. For recombination to occur, the unpaired electrons on the radical pairs must have opposing valence spins. These antiparallel spin states (singlet state) allow for rapid recombination. However, if the spin states are parallel (triplet state), then recombination cannot occur, and radical pairs diffuse away from one another. Modeling indicates some WMF strengths should promote the singlet state and recombination (thereby reducing ROS), while other strengths should promote the triplet state and diffusion (increasing ROS). Overall, these data suggest that in a field-strength dependent manner WMFs might be used for the directed manipulation of ROS.

However, the extant data on biological effects from WMFs often appears incongruent or contradictory. Exposure to WMFs has been shown to alter apoptosis, necrosis, and proliferation differently depending on tissue type in rat skeletal muscle *versus* renal cells [31]. Mouse embryonic stem cells exposed to 400 μT WMFs had increased levels of ROS and stimulated growth factors [32]. Fibrosarcoma cells exposed to only 0.2–2 μT WMFs also increased ROS levels, while conversely exposure to WMFs less than 3 μT reduced cell survival of mouse skeletal muscle [33, 34]. A recent study in planarians suggested that even at the same field strength, changes in frequency can lead to either inhibition, activation, or have no effect on regeneration [35]. These studies indicate that precise WMF exposures may hold the potential to be used as a novel therapeutic tool to control cell behaviors and alter tissue growth. But for a tool to be useful, it must be capable of inducing predictable effects on cell processes. Unfortunately, the lack of consistency in the methods and tissues/models used for studying WMF effects on tissue growth, combined with the absence of typical pharmacological dose response curves associated with WMF exposures, has made the practical usefulness of WMFs as a tool to manipulate growth unclear.

Previously, we established an animal model system for studying effects from WMF exposures on new tissue growth using the highly regenerative, free-living planarian flatworm *Schmidtea mediterranea*. In this study, we use this model to test several hypotheses based on the radical pair mechanism. Overall, we hypothesize that specific field strengths will predictably alter ROS signaling, suggesting WMFs can be used for the directed manipulation of stem cell behavior *in vivo*. Our first hypothesis is that WMF effects, as per the radical pair mechanism, occur largely through the modulation of radical pairs. This leads to the testable prediction that at different field strengths WMFs will produce opposite effects on ROS levels, resulting in a binary switch from decreased tissue growth to increased tissue growth. A second hypothesis we also test is that the cellular signaling downstream of ROS that controls stem cell proliferation is mediated by changes in H_2O_2, a product of O_2 metabolism and a common second messenger in ROS signaling (Figure 1B). These experiments aim to assess the potential for WMFs as a therapy and begin to dissect the mechanisms by which WMFs control stem cell-mediated tissue growth.

Planarians are a powerful model for investigating tissue growth mechanisms, as they can regenerate all tissues including the brain due in part to a massive population of pluripotent adult stem cells [36]. After a major injury, this stem cell population responds with increased proliferation and migration to the wound site, resulting in a blastema—undifferentiated new tissue comprised of stem cell progeny [37, 38]. Pharmacological inhibition of ROS blocks planarian regeneration, while activation of ROS signaling has been shown to rescue blastema formation [39, 40]. Previously, our own data demonstrated that in planarians ROS signaling is upregulated after injury and induces changes in gene expression that regulate the stem cell proliferation and differentiation required for blastema formation (Figure 1C), all of which were inhibited by exposure to 200 μT WMFs [15]. These experiments also indicated that at a different field strength (*e.g.*, 500 μT) tissue growth was instead increased, leading to our current hypothesis that these field strengths are predictably altering growth *via* changes in ROS signaling. Our current experiments reveal that exposure to different WMF strengths can be used to manipulate ROS signaling and stem cell behaviors in a predictable non-linear fashion to either inhibit or activate tissue growth. Furthermore, our data suggest that WMFs alter O_2^- and not H_2O_2 to modulate ROS signaling, providing direction for future studies.

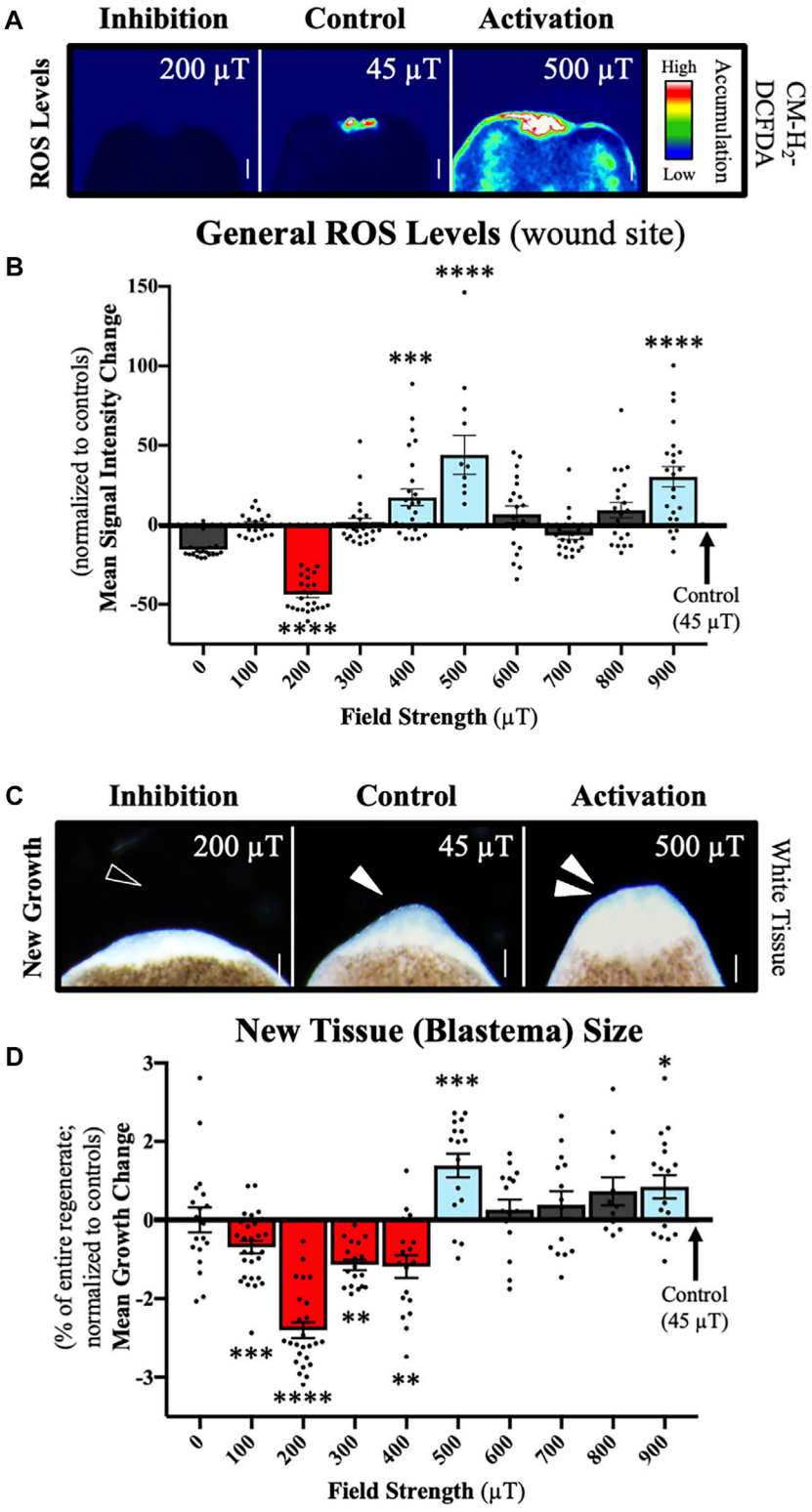

FIGURE 3
Weak Magnetic Fields (WMFs) Predictably Manipulate ROS Levels and Tissue Growth. Effects on planarian regeneration. **(A)** Representative field strength-dependent effects on ROS accumulation at the anterior wound site 1 h after injury, where 200 µT inhibits and 500 µT increases ROS levels as compared to 45 µT controls. ROS visualized with a general oxidative stress indicator fluorescent dye (CM-H_2DCFDA) as a heat map of signal intensity: red/white/green = high ROS; blue/black = low/none. **(B)** Quantification of **(A)** showing changes in ROS levels (as compared to 45 µT

(*Continued*)

FIGURE 3 (Continued)
controls) following exposure to 0–900 μT. n ≥ 12 for all strengths. (200 μT p = 0.0003; 400 μT p = 0.0025; 500 μT p = 0.0047; 900 μT p = 0.00013). 200 μT ROS data previously reported in (15). **(C)** Representative field strength-dependent effects on new tissue (blastema) size. The blastema is demarked by the white, unpigmented region, where 200 μT inhibits and 500 μT increases new tissue growth as compared to 45 μT controls (Earth normal = 25–65 μT). Anterior wound site shown at day 3 after injury. Empty arrow = inhibition. Solid arrow = normal blastema. Double solid arrows = increased blastema size. **(D)** Quantification of **(C)** showing changes in blastema size (as compared to 45 μT controls) after exposure to a range of field strengths from 0 −900 μT. Blastema size calculated as percent of entire regenerate size. n ≥ 11 for all strengths. (100 μT p = 0.0005; 200 μT p = 6.2205e-15; 300 μT p = 0.0056; 400 μT p = 0.0032; 500 μT p = 0.0003; 900 μT p = 0.0123). 0–600 μT blastema data previously reported in (15). For all: Anterior is up. Scale bars = 100 μm. Error bars = SEM. Red columns = inhibition. Blue columns = activation. Grey columns = no change. Significance: ANOVA with Tukey's post-hoc. *p < 0.05, **p < 0.01, ***p < 0.001, ****p < 0.0001.

Results

WMF effects are consistent with the radical pair mechanism

We experimentally controlled magnetic field exposure during planarian regeneration using a custom μ-metal enclosure (MagShield Box) to block external fields combined with Helmholtz coils to produce uniform magnetic fields at specific strengths (Figure 2). To test the hypothesis that different WMFs will produce opposite effects on new tissue growth that occur largely through modulation of radical formation, we examined both ROS accumulation and blastema formation following exposure to a controlled range of WMFs from 0 μT to 900 μT, in 100 μT increments (Figure 3). Controls were exposed to an Earth-normal 45 μT WMF, similar in strength to the geomagnetic field (which ranges from 25–65 μT). Planarian trunk fragments were created by transverse amputation just above and below the pharynx (removing both the head and tail) and regeneration was assessed at the anterior wound site. Trunk fragments were exposed to specific WMF strengths within 5 min of amputation and thereafter until analysis. The radical pair mechanism predicts that we should see some field strengths that increase as well as those that decrease ROS levels and regenerative growth.

ROS accumulation was assessed at 1 h after injury, when it has been shown that ROS is upregulated at the wound site [15]. To visualize ROS levels in live regenerates, we used a general oxidative stress indicator dye (CM-H_2DCFDA) that fluoresces upon ROS activity (Figure 3A). This allowed for the quantification of signal intensities and the statistical comparison of ROS accumulation at each field strength (Figure 3B). Our results show that compared to 45 μT controls, exposure to 200 μT WMFs prevented injury-induced ROS accumulation, while exposure to 400, 500, and 900 μT WMF exposures all caused significant increases in ROS levels. The greatest WMF effects were seen at 200 μT for inhibition and 500 μT for increased ROS accumulation.

Subsequent new tissue growth was assessed at 3 days after amputation, when blastema formation is considered complete [41]. The blastema is easily recognizable at this stage as white tissue at the wound site, since pigmentation has not yet occurred (Figure 3C). To account for any differences in worm size, blastema size was calculated as a percentage of total regenerate size (Figure 3D). We found that 100–400 μT exposures decreased blastema size, whereas at both 500 and 900 μT we observed the formation of larger than normal blastemas. Similar to our ROS findings, the greatest WMF effects on new tissue growth were seen at 200 μT for inhibition and 500 μT for increased blastema size. Our results demonstrate that WMFs can either increase or decrease both wound site ROS levels and tissue growth in a field strength-dependent manner.

These data suggest that a threshold potential exists to modulate tissue growth through WMF manipulation of ROS formation. Furthermore, they support 1) the hypothesis that WMF effects are consistent with our theoretical model, and 2) our hypothesis that WMF effects result mainly from the manipulation of ROS signaling. If correct, then we can predict equal and opposite changes in events mediated by ROS signaling, which in planarians includes control of adult stem cell behaviors after injury. Therefore, we next examined the effects of 200 and 500 μT WMFs (as representative of our observed effects) on ROS signaling and the resulting behaviors of stem cells during regeneration (Figure 4).

At 3 days after amputation, we investigated the expression of the chaperone heat shock protein 70 (Hsp70) (Figure 4A, top panels), which is involved in stress responses and cell survival [42, 43]. In planarians, blastema-associated *Hsp70* expression requires injury-induced ROS, and in turn *Hsp70* upregulation is required for ROS-mediated stem cell responses during regeneration [15, 44]. Therefore, at the same time point we also looked at the stem cell population using the general stem cell marker *Piwi*-1, as well as the late stem cell progeny marker *Agat*-1 (Figure 4A, middle panels). Our data showed that as predicted, as compared to controls, 200 μT WMFs caused a significant reduction in the expression of all three genes at the wound site, while 500 μT WMFs significantly increased expression (Figure 4B). These data demonstrate that WMF exposure can be used to directly inhibit or activate ROS signaling, depending on field strength.

Furthermore, we investigated WMF effects on proliferation at 3 h after injury (Figure 4A, bottom panels). In planarians, stem

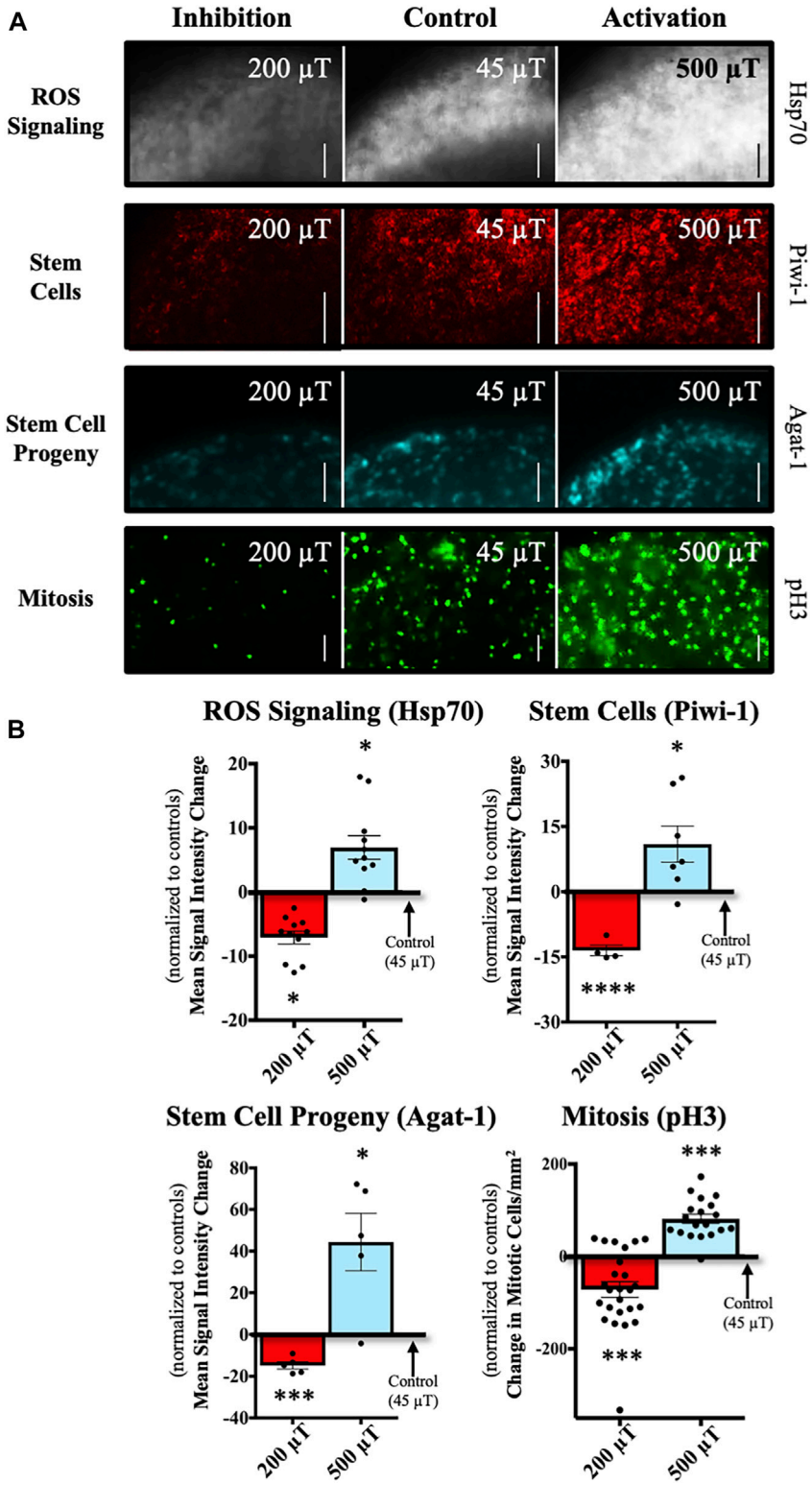

FIGURE 4
WMFs Predictably Manipulate ROS-Mediated Stem Cell Behavior. WMF effects (at the anterior wound site) from 200 µT or 500 µT exposure, as compared to 45 µT controls. **(A)** Representative images of stem cell markers and proliferation. Expression of heat shock protein 70 (Hsp70) at 3 days after injury (grayscale panels), a marker of ROS signaling during planarian regeneration. Piwi-1 expression at 3 days (red panels), a general marker of stem cells. Agat-1 expression at 3 days (cyan panels), a marker of late stem cell progeny (descendants). Actively dividing stem cells (mitosis) at
(*Continued*)

FIGURE 4 (Continued)
3 h (green panels), as revealed by phospho-histone 3 (pH3) labeling. **(B)** Quantification of **(A)** showing changes in expression/mitosis as compared to 45 μT controls. Hsp70, $n = 11$ (200 μT $p = 0.0299$; 500 μT $p = 0.0491$). Piwi-1, $n \geq 5$ (200 μT $p = 0.0008$; 500 μT $p = 0.0395$). Agat-1, $n \geq 7$ (200 μT $p = 0.0038$; 500 μT $p = 0.0281$). Mitosis, $n \geq 19$ (200 μT $p = 0.0005$; 500 μT $p = 0.0003$). For all: Anterior is up. Scale bars = 50 μm. Gene expression (mRNA) visualized by fluorescent *in situ* hybridization. Mitotic cells visualized by immunofluorescence. Error bars = SEM. Red columns = inhibition. Blue columns = activation. Significance: Student's *t*-test. *$p < 0.05$, ***$p < 0.001$, ****$p < 0.0001$.

cells have been found to be the only actively dividing cell population. Thus, we examined stem cell proliferation by looking at the presence of phosphorylated Histone H3 (pH3), which labels mitotically active cells. We found that at 200 μT there were significantly fewer mitotic cells, while at 500 μT there was a significant increase in the number of mitotic cells (Figure 4B). These results are consistent with our prediction that WMFs could both inhibit the activation of stem cell proliferation following injury as well as increase the proliferative response.

Together, our data indicate that exposure to WMFs produces non-stochastic changes that are predictable based on our theoretical principles (Figure 1A), which suggest that different field strengths have opposing effects. Furthermore, the data provide strong evidence that WMF effects on proliferation and tissue growth are consistent with the manipulation of ROS. These results support further investigation into the potential use of WMFs as a tool to alter stem cell activity.

Weak magnetic fields modulate superoxide levels

The majority of cellular ROS signaling is transduced by either H_2O_2 or O_2^- [45, 46]. In planarians, both H_2O_2 and O_2^- are present at the wound site following injury [47]. Therefore, we next sought to examine the effects of WMF exposures on these specific species (Figure 5). We hypothesized that WMFs modulate ROS signaling by influencing the formation of H_2O_2, since it has been well demonstrated as an ROS mediator of traditional signaling pathways.

To test this, we exposed regenerating planarians to 200 and 500 μT WMFs (with 45 μT controls) as before, and then examined the levels of H_2O_2 using the species-specific fluorescent reporter dye peroxy orange 1. Since with our general ROS indicator dye (Figure 3) we observed a peak at 1 h after injury, we chose that time point to examine H_2O_2 levels at the wound site (Figure 5A). However, there were no significant changes in the amount of H_2O_2 at either 200 or 500 μT (Figure 5B). In case there was a time delay in WMF effects specifically on H_2O_2, we also tested for effects at 2 h after injury but did not observe any significant changes (Figures 5A, B).

We then repeated these same analyses with the O_2^- specific fluorescent reporter dye orange 1. The data show that WMFs do alter wound site O_2^- levels at both 1 and 2 h after injury (Figure 5C). At 1 h, 200 μT WMF exposure significantly reduced O_2^- accumulation, although 500 μT produced no change; while at 2 h, 200 μT reduced and 500 μT increased levels of O_2^- at the wound site (Figure 5D). This pattern of opposing inhibition and activation of O_2^- by WMFs mirrored our results seen from WMF effects on ROS-mediated stem cell activity (Figure 4). However, these results were inconsistent with our hypothesized role for H_2O_2 in mediating WMF effects during tissue growth.

Studies suggest that H_2O_2 signaling plays a role during planarian regeneration [15, 39, 40, 47]. Therefore, we further investigated the possible differential roles for H_2O_2 and O_2^- in mediating the effects of WMFs on planarian regeneration (Figure 6). The general flavoenzyme inhibitor diphenyleneiodonium chloride (DPI) is often used as a pharmacological NADPH oxidase inhibitor [48, 49]. To confirm a role for H_2O_2 during regeneration, we examined the ability of exogenous H_2O_2 (which is cell permeable and readily diffuses across the plasma membrane) to rescue tissue growth following general ROS inhibition by DPI (Figures 6A–C). We pre-exposed animals to either 10 μM DPI or its vehicle control dimethyl sulfoxide (DMSO), amputated to produce trunk fragments, then allowed fragments to regenerate without drug exposure. At 3 days after amputation, blastema formation was significantly inhibited, while the addition of 400 μM H_2O_2 after amputation was able to rescue/overcome this chemical block of ROS (Figure 6C).

We repeated this H_2O_2 rescue assay but following inhibition of ROS by 200 μT WMF exposure, and without any pre-exposure before amputation (Figures 6D–F). Unlike chemical ROS inhibition, we found that WMF inhibition of blastema formation at 3 days could not be rescued by the addition of H_2O_2 (Figure 6F). To further support these findings, we also analyzed the effects of exogenous H_2O_2 on O_2^- levels without experimentally controlled WMF exposure (Figures 6G–I). Adding H_2O_2 alone, even with adding a 24 h pre-treatment, failed to significantly affect injury-induced O_2^- levels at the wound site at 2 h after injury (Figure 6I). As our results reveal that exposure to WMFs was able to alter the injury-induced accumulation of O_2^- at this same time point, the data suggest that WMF effects

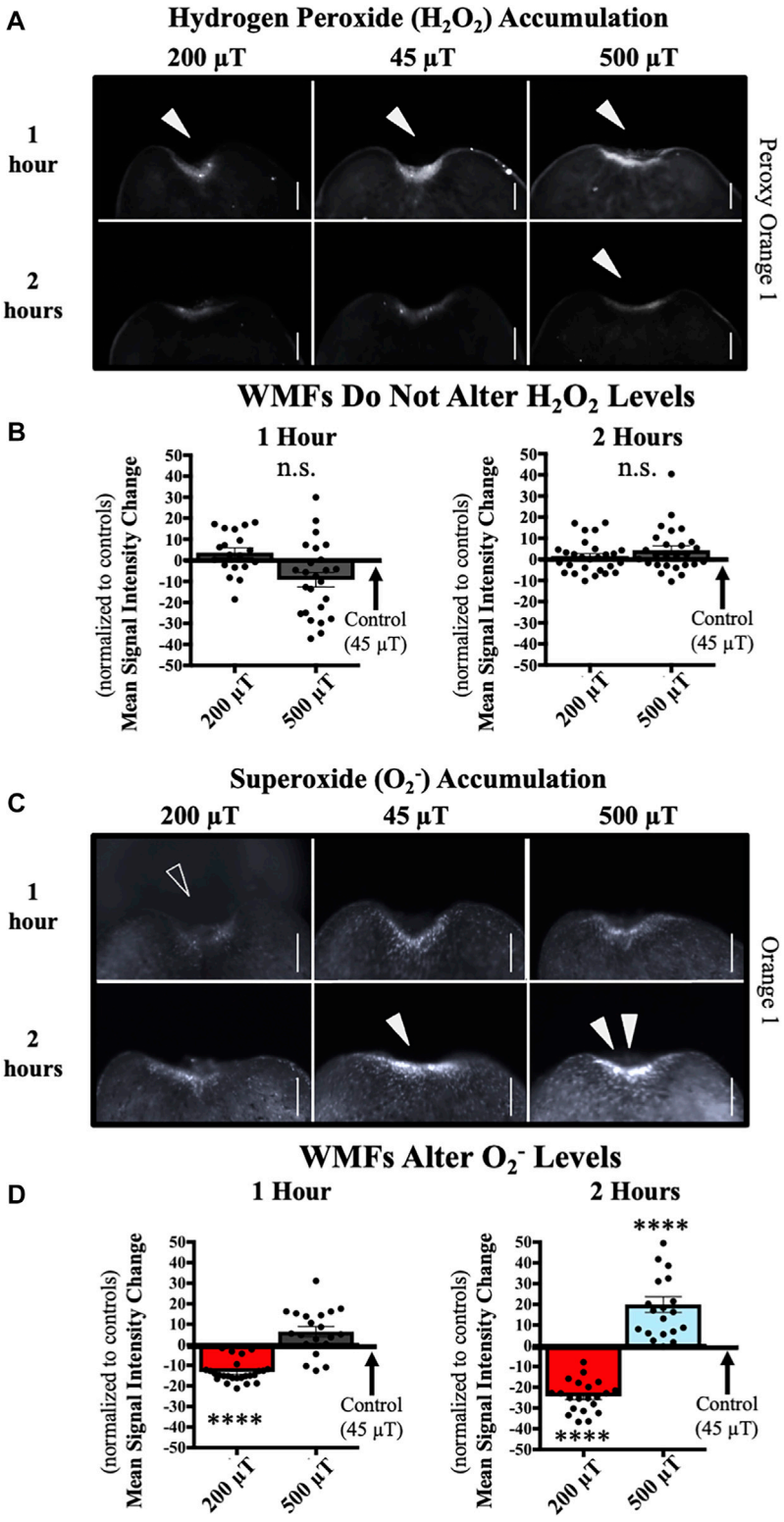

FIGURE 5
WMFs Alter Superoxide (O_2^-) but not Hydrogen Peroxide (H_2O_2) Levels. WMF effects (at the anterior wound site) from 200 µT or 500 µT exposure (as compared to 45 µT controls), as shown at 1 h and 2 h after injury. **(A)** H_2O_2 accumulation visualized by peroxy orange 1 live fluorescent dye. Solid arrows = peak of accumulation. **(B)** Quantification of **(A)**, showing no change in levels as compared to 45 µT controls. n ≥ 19. n.s. = not significant. **(C)** O_2^- accumulation visualized by orange 1 live fluorescent dye. Open arrow = loss of accumulation. Solid arrow = peak of
(*Continued*)

FIGURE 5 (Continued)
accumulation (note lack of peak at 2 h with 200 μT). Double solid arrows = increased accumulation (note lack of increased accumulation at 1 h with 500 μT). **(D)** Quantification of **(C)** showing changes in levels as compared to 45 μT controls. (At 1 h: 200 μT p = 6e-9; at 2 h 200 μT p = 2e-7 and 500 μT p = 0.00009). For all: Anterior is up. Scale bars = 100 μm. Error bars = SEM. Red columns = inhibition. Blue columns = activation. Grey columns = no change. Significance: Student's t-test. ****$p < 0.0001$.

on tissue growth do not occur *via* H_2O_2, but instead are O_2^-—mediated.

Species-specific ROS accumulations at wounds are temporally distinct

During our investigation into the effects of specific WMFs on H_2O_2 and O_2^- levels at the wound site, we noticed there appeared to be a difference in levels of individual species accumulation at 1 h *versus* 2 h. Furthermore, in these WMF experiments the apparent pattern of peak species accumulation seemed to differ between H_2O_2 and O_2^- (Figure 5). To better probe the temporal kinetics of ROS accumulation without confounding variables, we investigated normal H_2O_2 and O_2^- levels during tissue growth without experimentally controlled WMF exposure (Figure 7). Our data show that peak H_2O_2 accumulation after injury occurred at 1 h, with a significant decrease by 2 h. Conversely, while O_2^- was present at the wound site by 1 h, O_2^- levels did not peak until 2 h.

During metabolism, O_2^- is converted into H_2O_2 by the enzyme superoxide dismutase (SOD), which effectively increases H_2O_2 levels by reducing O_2^- levels (Figure 1B). If this enzymatic pathway is a main driver of ROS signaling during tissue growth, then we would predict that O_2^- accumulation would temporally precede H_2O_2 accumulation. Instead, our data indicate that H_2O_2 levels peak before O_2^- levels peak. Separately from its interaction with SOD, O_2^- also interacts with nitric oxide (NO) to form peroxynitrite ($ONOO^-$), which (like H_2O_2) is known to control traditional cell signaling pathways downstream of O_2^- levels [50, 51].

Therefore, we next hypothesized that instead of driving H_2O_2 formation, O_2^- reacts with NO to promote $ONOO^-$ signaling. If supported, we would predict that 1) injury-induced wound site $ONOO^-$ accumulation occurs during planarian regeneration, and 2) the pattern of peak $ONOO^-$ levels would align temporally with our observed peak of O_2^-. We used the species-specific fluorescent reporter dye 2′,7′-dichlorodihydrofluorescein diacetate (DCDHF) to visualize $ONOO^-$ levels during tissue growth (Figure 7A, bottom panels). Our data show that similar to O_2^-, while at 1 h $ONOO^-$ was present at the wound site, there was a significant increase in $ONOO^-$ levels by 2 h (Figure 7B).

Together, these data reveal that the accumulation of H_2O_2 and O_2^- are temporally distinct during stem-cell mediated tissue growth. In addition, our results highlight a previously unappreciated role for H_2O_2-independent ROS signaling mechanisms during this process. These data indicate that both H_2O_2 and O_2^-/$ONOO^-$ pathways are activated after injury, suggesting that ROS mechanisms during planarian regeneration are reliant on more than one ROS signaling pathway.

Discussion

The study of ROS across various developmental, regenerative, and disease model systems has resulted in an explosion of data revealing the importance of this highly reactive group of oxygen-containing molecular products. In searching for ways to exert control over the vast array of cellular functions that ROS influences, researchers have turned to exploring multiple modalities. Exposures to moderate and strong magnetic fields are known to affect radicals and biological processes [52]. However, the research on WMFs (including ours) indicates that field strengths below 1 mT have important biological implications as well. While the potential of WMF exposure as a non-invasive means to control stem cell activity and cell proliferation is exciting, enthusiasm for being able to translate this potential into real-world approaches is dampened by the need to address gaps in our fundamental understanding of the mechanisms involved.

The work presented here aims to begin addressing these gaps by testing several simple, but critical, current hypotheses in the field. The first was that WMF effects, while not following the conventional dose response curves of pharmacological treatments, can be predicted based on theoretical models and therefore represent a potential tool for the directed manipulation of cell proliferation and tissue growth. The second hypothesis followed from the first, given our predictions were based on the radical pair mechanism: that the effects of WMFs during tissue growth are due largely to modulation of ROS signaling. This mechanism predicts that at different field strengths WMFs will produce opposite effects on ROS levels, resulting in a non-linear (binary) switch from decreased tissue growth to increased tissue growth. If supported, this could help explain why the data reported in the literature for effects from WMFs can often appear contradictory. Not only are the effects likely context dependent (as are most treatments) but vary by field strength. In addition, WMF effects would also be determined in part by the different outcomes associated with individual threshold levels for free radicals such as ROS and reactive nitrogen species (RNS;

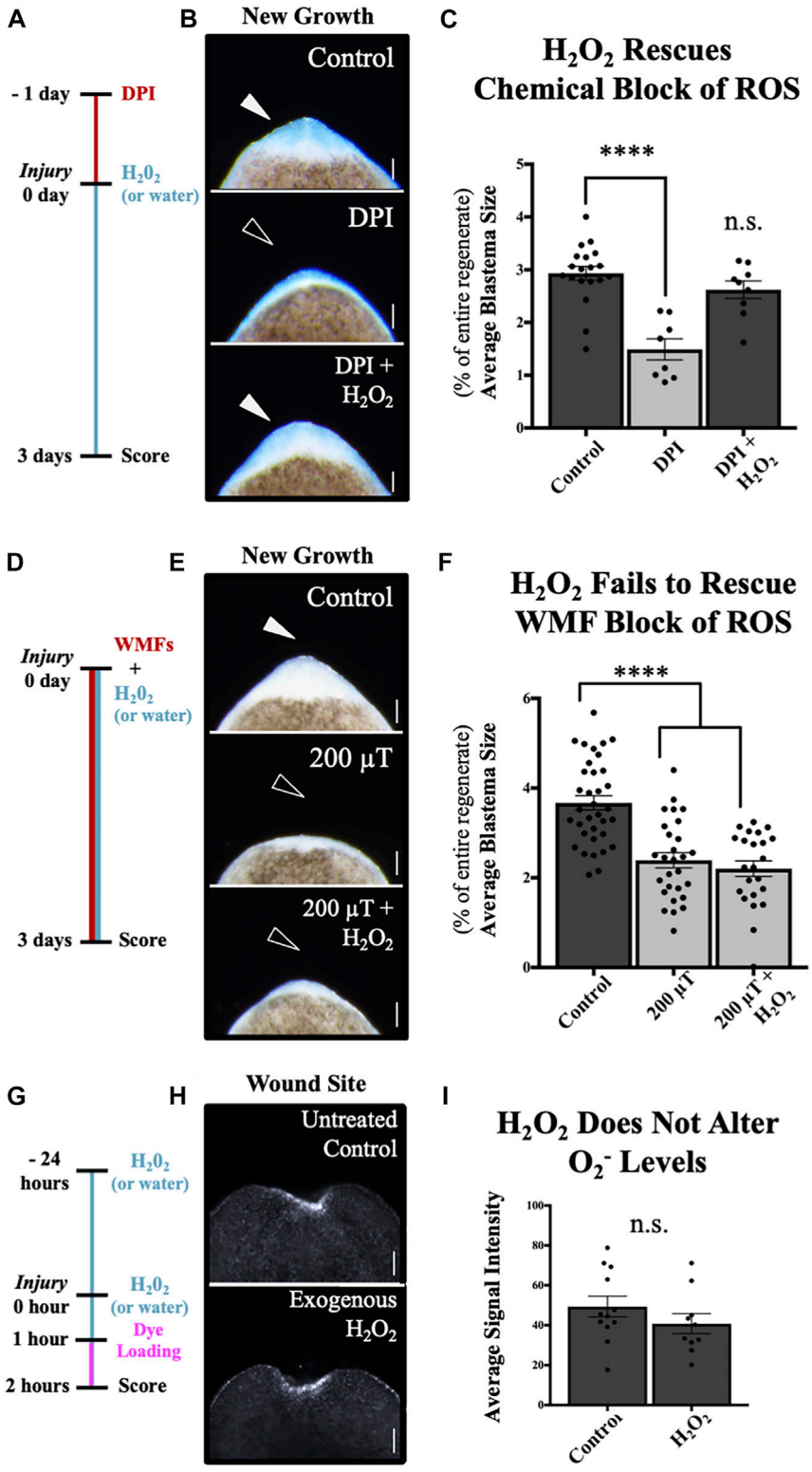

FIGURE 6
H_2O_2 Rescues Chemical, but not WMF, Inhibition of Tissue Growth. New tissue and superoxide levels at the anterior wound site. **(A–C)** Blastema size at 3 days post injury after chemical inhibition of ROS by 10 µM diphenyleneiodonium (DPI), an NAD(P)H oxidase inhibitor. **(A)** Treatment scheme. Animals were pre-treated for 24 h prior to injury, then amputated. All regenerates were returned to untreated worm water, except for DPI + H_2O_2 animals, which were then placed in 400 µM H_2O_2 until scoring. Controls = vehicle control (DMSO only). **(B)** Images of new tissue growth. **(C)**
(*Continued*)

FIGURE 6 (Continued)
Quantification of **(B)**. n ≥ 8. (DPI p = 0.00004). **(D–F)** Blastema size at 3 days post injury after WMF inhibition of ROS by 200 μT. **(D)** Treatment scheme. All animals were exposed to the specified WMF immediately after amputation. 200μT + H_2O_2 animals were also placed in 400 μM H_2O_2 at that time. Controls = 45 μT exposure only (Earth normal). **(E)** Images of new tissue growth. **(F)** Quantification of **(E)**. n ≥ 23. (200 μT p = 7.47e-7; 200μT + H_2O_2 p = 3e-9). **(G–I)** O_2^- levels at 2 h post injury visualized by orange 1 live fluorescent dye. Note: these animals were not exposed to specific WMFs but placed in a temperature-controlled incubator as standard for the field. **(G)** Treatment scheme. Exogenous H_2O_2 animals were pre-treated with 400 μM H_2O_2, then after injury returned to fresh H_2O_2 for 1 h prior to being placed in O_2^- specific dye for another hour. Controls = untreated (kept in normal worm water up until dye loading). **(H)** Images of wound site at 2 h. **(I)** Quantification of **(H)**. n ≥ 10. n.s. = not significant. For all: Anterior is up. Scale bars = 100 μm. Solid arrows = control blastema size. Open arrows = inhibition. Error bars = SEM. Dark grey columns = control values. Light grey columns = inhibition. Significance: Student's t-test. ****$p < 0.0001$.

another class of molecules involved in cell signaling), which have both been implicated in a wide array of biological systems [53, 54].

Our data demonstrate that consistent with the radical pair mechanism, the effects of WMFs across a range of field strengths can be predicted by the known outcomes of ROS signaling at given threshold levels. Thus, unlike many molecular-genetic tools, WMFs can be used to direct biological outcomes for both loss- and gain-of-function depending on the field strength used. Our data show that exposure to 500 μT WMFs increased ROS accumulation, resulting in upregulated gene expression, increased proliferation, and expansion of stem cell and progeny cell populations—all of which result in increased tissue growth. And (as further predicted by our theoretical model) exposure to 200 μT resulted in the opposite effect, blocking stem cell-mediated new growth as a result of inhibiting ROS accumulation after injury.

WMFs have been shown to alter ROS levels and cell behaviors *in vitro* under context-specific circumstances, and these effects are often attributed to the radical pair mechanism [55]. For example, WMF strengths ranging from 0 to 600 μT were shown to either inhibit or promote growth and ROS levels in fibrocarcinoma cell culture depending on field strength [56]. Both RNS and ROS signaling are important regulators of stem cells, proliferation, cell migration, and tissue growth, where they can act as extracellular chemical cues as well as intracellular second messengers [57, 58]. For example, in bone marrow stem cells it was found that the addition of exogenous H_2O_2 prevented proliferation and differentiation [59], while an earlier study on RNS signaling showed that NO plays a critical role in cell differentiation [60].

During regeneration specifically, many studies (including in axolotl, zebrafish, *Xenopus*, and planarians) have identified ROS signaling as necessary to drive regenerative outgrowth [11, 39, 61, 62]. Others have shown that ROS is able to rescue pharmacologically inhibited regeneration, including a study in zebrafish that found exogenous H_2O_2 was sufficient to rescue heart regeneration [63]. For the present work, we hypothesized that WMF effects on stem cells were mediated by H_2O_2 specifically. There is ample evidence that H_2O_2 signaling plays an active role in planarian regeneration. H_2O_2 is upregulated at all wound sites within the first hour [40, 47]. The ROS inhibitor DPI inhibits both blastema formation and wound site H_2O_2 accumulation [15, 39, 40]. Furthermore, exogenous H_2O_2 has been shown to rescue regeneration in planarians with inhibited extracellular regulated kinase (ERK) signaling [40].

We were surprised to find that the data were not consistent with our hypothesis but instead indicate that O_2^- mediates our observed WMF effects. These results do not contradict an endogenous role for H_2O_2 during planarian regeneration. Instead, our findings suggest that 1) there is a previously unrecognized role for O_2^- signaling during planarian regeneration, and 2) that WMFs manipulate stem cell activity by modulating levels of O_2^- (Figure 8). Interestingly, data from our previous work support these findings [15]. There, we used RNA interference to knockdown superoxide dismutase (SOD), an enzyme that converts O_2^- into H_2O_2 [66], to rescue blastema growth in 200 μT exposed regenerates by increasing ROS levels. This loss of SOD not only rescued regeneration but in controls also resulted in increased blastema sizes [15], similar to our 500 μT WMF exposures. Importantly, loss of the SOD enzyme increases O_2^- levels at the expense of H_2O_2 levels. This provides support for our conclusion that the processes being affected by WMFs are not mediated by H_2O_2, highlighting the importance of O_2^- as a signaling molecule during regeneration.

Both O_2^- and H_2O_2 are known to transduce ROS signaling, with each independently regulating downstream signaling pathways (Figure 8A). Several oxygen- and nitrogen-containing molecules can act as second messengers, which typically transduce extracellular signals into a cellular response, including NO and $ONOO^-$. H_2O_2 acts as a second messenger to directly interact with downstream pathway members, while O_2^- can signal by either oxidizing proteins directly or by interacting with NO to form $ONOO^-$ [67]. Cellular O_2^- production occurs as a result of electron leakage from the mitochondrial electron transport chain, as well as through decoupled endothelial nitric oxide synthase (eNOS) reactions [64]. Moreover, coupled eNOS reactions are one major source of intracellular NO, which is required for the production of $ONOO^-$ [51]. While O_2^- can lead to the production of both $ONOO^-$ and H_2O_2, the formation of ONOO- *via* a NO is kinetically favored over the enzymatic conversation of O_2^- to H_2O_2 by SOD [68].

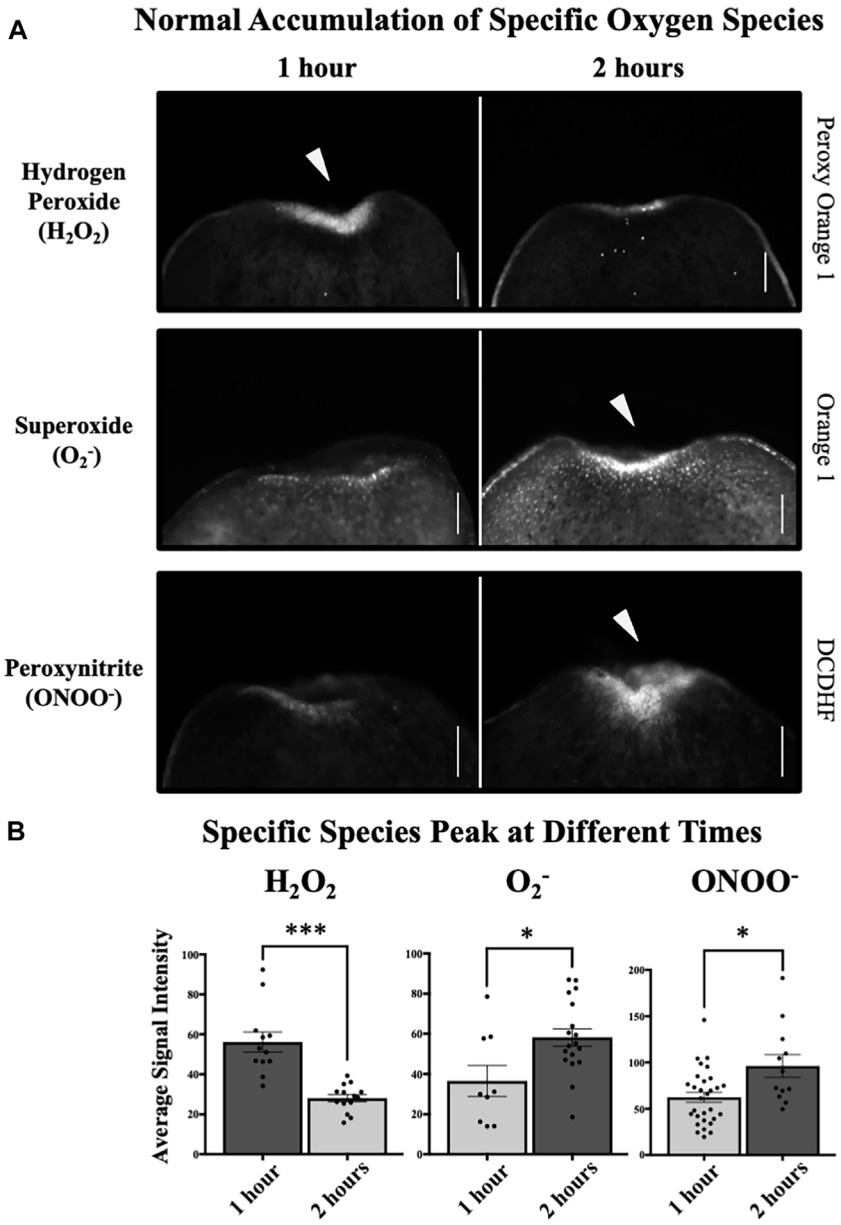

FIGURE 7
Induces Peaks of Hydrogen Peroxide (H_2O_2), Superoxide (O_2^-), and Peroxynitrite ($ONOO^-$). Species accumulation at 1 h and 2 h post injury at the anterior wound site, visualized by species-specific live fluorescent dyes. Note: these animals were not exposed to specific WMFs but placed in a temperature-controlled incubator as standard for the field. **(A)** Normal accumulation of specific oxygen species. H_2O_2 levels as visualized by peroxy orange 1. O_2^- levels as visualized by orange 1. $ONOO^-$ levels as visualized by 2′,7′-dichlorodihydrofluorescein diacetate (DCDHF). **(B)** Quantification of **(A)** showing H_2O_2 levels peak at 1 h, while both O_2^- and $ONOO^-$ levels peak at 2 h. H_2O_2, $n \geq 12$ ($p = 0.00012$). O_2^-, $n \geq 9$ ($p = 0.0285$). $ONOO^-$, $n \geq 12$ ($p = 0.0232$). For all: Anterior is up. Scale bars = 50 μm. Solid arrows = peak of accumulation. Error bars = SEM. Dark grey columns = peak levels. Light grey columns = non-peak levels. Significance: Student's *t*-test. *$p < 0.05$, ***$p < 0.001$.

ONOO- signaling is known to be upstream of cell fate decisions; in neural stem and progenitor cell populations ONOO- has been shown to regulate stem cell renewal and proliferation [69, 70]. While our data did not reveal any regulation of O_2^- levels by H_2O_2, crosstalk between the two pathways does exist. In fact, the inactivation of SOD and thus reduced production of H_2O_2 occurs as a direct result of $ONOO^-$ formation after a NO and O_2^- reaction [71]. Our data indicate that both O_2^- and H_2O_2 mediate ROS signaling during planarian regeneration, but that WMFs affect O_2^- signaling specifically. This is reinforced by our finding that following injury the peak of H_2O_2 is WMF insensitive,

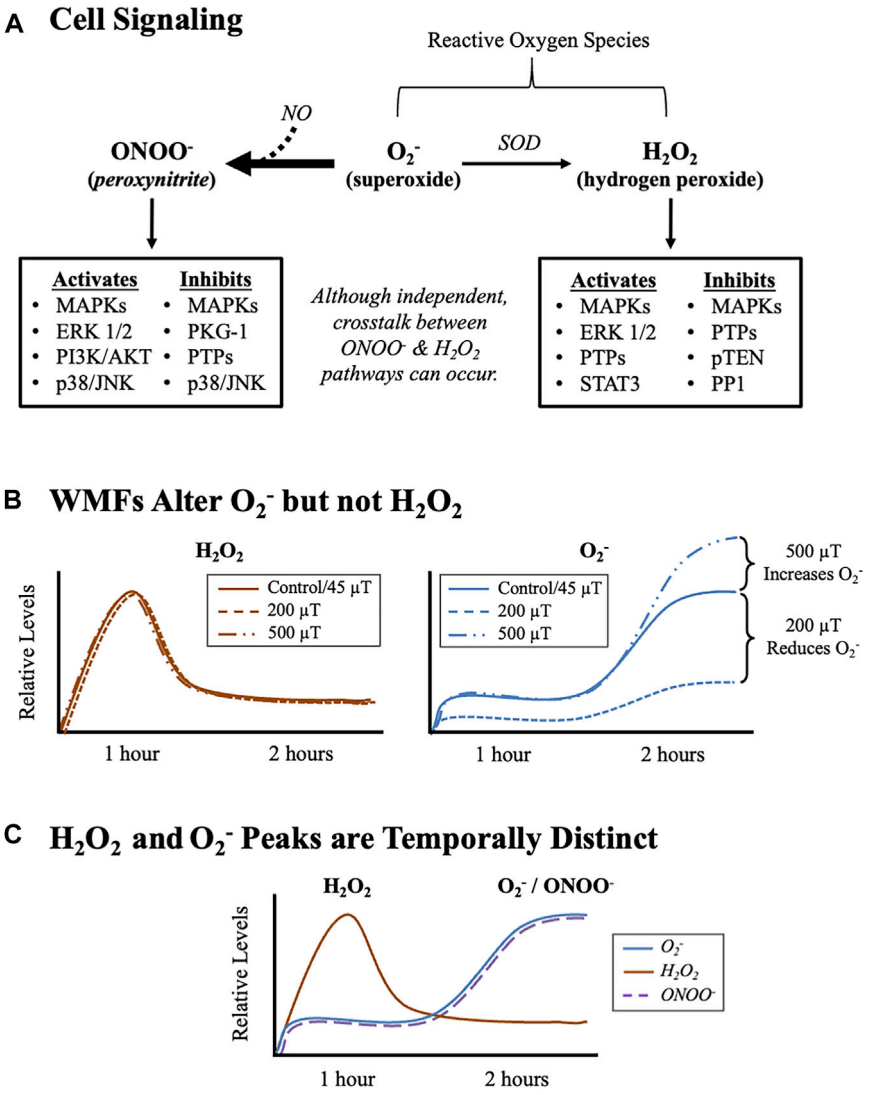

FIGURE 8
WMFs Modulate Stem Cell Behavior Via the Pleiotropic Signaling Molecule, Superoxide (O_2^-). **(A)** Cell signaling pathways downstream of oxygen containing molecules and their relationship to O_2^-. Note: although H_2O_2 signaling and O_2^-/$ONOO^-$ signaling are regulated independently, there can be tissue/organ/organism-specific crosstalk between them. MAPK (mitogen activated protein kinase) signaling includes: ERK 1/2 (extracellular regulated kinase 1/2), p38, and JNK (c-Jun-N terminal kinase). Other effectors include: PI3K/AKT (phosphatidylinositol-3-kinase/Akt serine/threonine kinase family) signaling; PI3K/AKT (phosphatidylinositol-3-kinase/Akt serine-threonine kinase family) signaling; cyclic GMP-dependent kinases, like PKG-1 (protein kinase G-1); protein tyrosine phosphatases (PTPs); the serine/threonine phosphatase PP1 (protein phosphatase 1); the protein and lipid phosphatase pTEN (phosphatase and tensin homolog deleted on chromosome 10); and the JAK-STAT (janus kinase-signal transducer and activator of transcription) pathway member STAT3. For more information, please see reviews of O_2^- metabolism [64], $ONOO^-$ signaling [65], and H_2O_2 signaling O_2^- [45]. **(B)** Graphical summary of our WMF experimental data. Relative changes in H_2O_2 (orange) and O_2^- (blue) values after WMF exposures (see data Figure 5). Note that WMFs only affect O_2^- levels. **(C)** Graphical summary of normal accumulation of oxygen containing molecules after injury. Relative changes in H_2O_2 (orange), O_2^- (blue), and $ONOO^-$ (dashed purple) during planarian regeneration in the absence of experimentally-controlled WMF exposure (see data Figure 7). Note that O_2^- and $ONOO^-$ both peak 1 h after H_2O_2 peaks.

whereas the peak of O_2^- can be inhibited by 200 µT and increased by 500 µT WMFs (Figure 8B). Furthermore, our data demonstrate that these peaks are temporally distinct, with peak H_2O_2 levels occurring at 1 h after injury and peak levels of both O_2^- and $ONOO^-$ occur subsequently at 2 h after injury (Figure 8C).

This temporal shift in species' peaks suggest that there may be a difference in the temporal requirement for H_2O_2 *versus* O_2^-/$ONOO^-$ signaling. This is supported by our findings that peak O_2^-/$ONOO^-$ levels occur *after* H_2O_2 levels peak. In further support of this, our previous work demonstrated that 200 µT WMF exposures are still able to inhibit tissue growth if the start

of the exposure is delayed until after the H_2O_2 peak [15]. These results demonstrate that presence of the 1 h post injury H_2O_2 peak is not able to rescue regeneration with WMF inhibition of tissue growth. Together, the data suggest that injury-induced H_2O_2 signaling may play an earlier role during tissue growth (such as during initiation of regeneration), while O_2^-/$ONOO^-$ signaling functions independently at later time points (for example, as a propagation signal to maintain growth). This is a future direction that we will be investigating.

Although the studies presented here did not address the role of cell migration on WMF effects during tissue growth, it is interesting to note that the migration of planarian stem cells and their progeny to the wound site and into the forming blastema does occur [72, 73]. While wound closure is typically completed by 1 h post injury, migration to the wound site is known to occur later and be sustained during blastema formation. ROS in general and superoxide specifically have been shown to promote cell migration in multiple other contexts [74–76], which suggests the possibility that in planarians WMF effects might potentially include changes in ROS-mediated cell migration. However, since superoxide regulation of cell migration has commonly been shown to occur *via* SOD-induced increases in H_2O_2 signaling [77, 78], and since RNS signaling has been shown to be a negative regulator of cell migration [79, 80], this area of inquiry would require a great deal more investigation.

RNS have emerged as vital components of the wound healing process, which occurs prior to and is closely tied to tissue regeneration in many species [81, 82]. For example, NO has been shown to enhance wound healing in diabetic chronic wounds by accelerating cell proliferation and migration after injury [83], and as such NO donors are promising candidates for use in hydrogels to treat wounds [84]. However, like ROS, both too much and too little RNS can be harmful. And while both ROS and RNS have been shown to play roles during cell proliferation and new tissue growth, the mechanisms of RNS signaling during regeneration are much less well understood [85, 86]. Although a recent study has demonstrated a role for NO during zebrafish fin regeneration [87], the role of RNS in the regenerative process is still largely uncharacterized and its role during planarian regeneration is currently unknown. Given the potential, based on the radical pair mechanism, for WMF interactions with RNS signaling during tissue growth, this is a promising area for further studies.

Moving forward, elucidation of the underling mechanisms governing the behavior of quantum phenomena in biological systems will be vital. Mounting evidence on the effects of WMFs highlight the possibilities for exposures to elicit control over disease states *via* ROS. In cancer research, ROS are of increasing interest as a therapeutic target and data suggest tumor cells may be more sensitive to minor changes in ROS levels than other cell types [88, 89]. In the immune system, upregulation of ROS is essential to host defenses against bacterial infection, where neutrophils release high levels of ROS at the site of infection [90]. Furthermore, autoimmune diseases, such as multiple sclerosis, are associated with significantly increased ROS levels, which are thought to participate in provoking the autoimmune response [91]. Therefore, research into the mechanisms that govern the effects of WMFs on biological systems holds the potential to unlock new and innovative therapies in areas of regenerative medicine, cancer research, and more.

Methods

Animal care and amputations

The asexual clonal line of *Schmidtea mediterranea* (CIW4) was maintained in the dark at 18 C. Planarians were kept in ultrapure Type 1 water with Instant Ocean salts at 0.5 g/L (worm water). Animals were fed every third week with liver paste processed from a whole calf liver (antibiotic and hormone free) obtained from Creekstone Farms (Arkansas City, KS). Liver paste was never frozen or thawed more than once before feedings. Worms 2–5 mm in length were used for all experiments and worms were starved at least 1 week before use. Amputations were done as previously described [92] with a dissecting microscope on a custom-made cooling Peltier plate. Trunk fragments were produced *via* transverse amputation just anterior and posterior to the pharynx, with cuts made at a 90 degree angle to the sagittal plane for consistency in wounding. All untreated controls were held according to field standards in a biological oxygen demand incubator (VWR) at 18 C in the dark.

Magnetic field exposures

Experimentally-controlled static WMF exposures were done with custom-built triaxial Helmholtz coils in a μ-metal enclosure (MagShield box) to block external magnetic fields as previously described [15]. Direct electric current to Helmholtz coils was supplied by DC power sources (Mastech HY3005D-3) and was fed through both *x* and *y* axis coils to produce a uniform magnetic field. The MagShield box was kept in a temperature-controlled room (20 C). Animals were placed in either 35 or 60 mm Petri dishes in worm water (or in specific media as described in individual assays) in the center of each Helmholtz coil. Magnetic field exposures were performed in the dark always with one coil set at 45 μT (Earth normal average for the geomagnetic field) separated by a μ-metal partition from the other side, where a second coil was set at indicated experimental field strengths from 0 to 900 μT. Before and at the end of each experiment field strengths were confirmed using either a gauss or mG m (AlphaLab models GM1-HS or MGM). Unless otherwise specified, all planarians were exposed

to WMFs within 5 min of amputation and then continuously until scoring and imaging at the indicated time. For Figure 3D: total experimental replicates for blastema growth assays were n ≥ 1, with total biological replicates for each condition as follows: 45 μT, n = 164; 0 μT, n = 19; 100 μT, n = 28; 200 μT, n = 25; 300 μT, n = 18; 400 μT, n = 18; 500 μT, n = 17; 600 μT, n = 16; 700 μT, n = 14; 800 μT, n = 11; 900 μT, n = 18.

Detection of reactive oxygen species and oxygen-containing molecules

General ROS and individual species were visualized by the use of cell-permeant live fluorescent reporter dyes. All images were taken ventrally, and animals were kept in the dark while loading dye. For detecting general ROS levels, the oxidative stress indicator dye, 5-(and-6-)-chloromethyl-2',7′-dichlorodihydrofluorescein diacetate (CM-H_2DCFDA; Molecular Probes C6827; excitation, 470 nm; emission, 525 nm) was used. Intact planarians were pre-exposed to the specified WMFs (see above) for 23 h*, at which time they were amputated to produce trunk fragments. Fragments were placed in 25 μM CM-H_2DCFDA (from 10 mM DMSO stock) and returned to the specified WMF for 1 h, at which time regenerates were rinsed 3X in worm water and imaged. Total experimental replicates were $n \geq 1$. Total biological replicates were: 45 μT, n = 189; 0 μT, n = 19; 100 μT, n = 17; 200 μT, n = 24; 300 μT, n = 23; 400 μT, n = 26; 500 μT, n = 12; 600 μT, n = 20; 700 μT, n = 22; 800 μT, n = 21; 900 μT, n = 23. (*Note, we have since determined that WMF pre-exposure is not required to obtain the observed WMF effects; see for example our H_2O_2 and O_2^- WMF data in Figure 5 and Figure 6D–F)

This protocol was used for the remaining dyes, with the following exceptions: H_2O_2 was detected by soaking newly amputated fragments (with no WMF pre-exposure) in 20 μM peroxy orange 1 (Sigma SML0688; from 1 mM DMSO stock; excitation, 470 nm; emission, 525 nm) plus the specified WMF for 1-h prior to imaging. O_2^- was detected by soaking fragments (with no WMF pre-exposure) for 1-h prior to imaging in 2 μM orange 1 (Enzo Life Sciences ENZ-51012; from 5 mM dimethylformamide stock; excitation, 550 nm; emission, 620 nm). For "normal" (untreated/unexposed) experiments, peroxy orange 1 and orange 1 dye were used as above, but without concurrent WMF exposure. $ONOO^-$ was detected by soaking regenerating fragments in 10 μM 2′,7′-dichlorodihydrofluorescein diacetate (DCDHF) for 1-h prior to imaging (Enzo life sciences ALX-610-022-M050; from 10 mM dimethylformamide stock; excitation 502 nm; emission 523 nm). For 2 h timepoints, fragments were cut and allowed to regenerate for 1 h, at which time animals were soaked in dye for another hour before rinsing and imaging. For all time points, animals were rinsed in ice cold worm water 3X to preserve fluorescence. Total experimental replicates for all were $n \geq 2$. Total biological replicates for O_2^- were: 45 μT at 1 h, n = 42; 200 μT at 1 h, n = 25; 500 μT at 1 h, n = 20; untreated at 1 h n = 9; 45 μT at 2 h, n = 53; 200 μT at 2 h, n = 21; 500 μT at 2 h, n = 20; untreated at 2 h, n = 18. Total biological replicates for H_2O_2 were: 45 μT at 1 h, n = 47; 200 μT at 1 h, n = 19; 500 μT at 1 h, n = 25; untreated at 1 h, n = 12; 45 μT at 2 h, n = 58; 200 μT at 2 h, n = 27; 500 μT at 2 h, n = 26; untreated at 2 h, n = 14. Total biological replicates for $ONOO^-$ were: untreated at 1 h, n = 30; untreated at 2 h, n = 12.

Immunostaining and *in situ* hybridization

Fluorescent *in situ* hybridization (to observe and quantify mRNA expression) was performed as previously described [93], with the following exceptions: Prehybe and hybe used yeast RNA at 1 mg/ml and probe dilution was 0.5 ng/μl with hybridization for 24 h. *S. mediterranea* riboprobes to Hsp70, Piwi-1, and Agat-1 were generated as described in our previous paper in (15). The regions/primers used were: for Hsp70, a 552 bp region from 5′-GGTTTTTGATTTGGGTGGTG to 3′-AGCTGTTGCTATGGGAGC; for Piwi-1, a 2461 bp region from 5′-GATCCCAATTTAAGACCAAGAAGAG to 3′-TTTTTATGTATTCGATTAAAAAAAA; and for Agat-1, 404 bp from 5′-GGAGTTAAAGTGTCCATCCAG to 3′-GTTGCTAACCTGACTGACATGC. Total experimental replicates for all were $n \geq 1$. Total biological replicates for Hsp70 riboprobe were: 45 μT, n = 11; 200 μT, n = 11; 500 μT, n = 11. For Piwi-1 riboprobe: 45 μT (200 μT control), n = 4; 200 μT, n = 4.45 μT (500 μT control), n = 7; 500 μT, n = 7. For Agat-1 riboprobe: 45 μT (200 μT control), n = 5; 200 μT, n = 5; 45 μT (500 μT control), n = 5; 500 μT, n = 5. Labeling of miotic cells by immunostaining was performed as previously described [94], with anti-pH3 (Sigma/Millipore 04-817; 1:25) as the primary antibody. A goat anti-rabbit horseradish peroxidase (Invitrogen 65-6120) with TSA Cyanine 3 (Cy3)-tyramine (PerkinElmer; 1:50) amplification was used as the secondary antibody. All experiments were run once with controls. For Piwi-1 and Agat-1 a second experiment was run for representative photos. Total biological replicates: 45 μT, n = 39; 200 μT, n = 25; 500 μT, n = 19.

Pharmacology

ROS production was inhibited with diphenyleneiodonium chloride (DPI; Sigma D2926). Endogenous ROS in the form of H_2O_2 was administered by soaking planarians in 400 μM H_2O_2 (diluted from 30% stock; Sigma 216763). For Figures 6A–C: Intact worms were presoaked in 10 μM DPI (from 1 mM DMSO stock) for 24 h. Animals were amputated to form trunk fragments, then placed in worm water (DPI) or

400 μM H_2O_2 (DPI + H_2O_2) and allowed to regenerate at 18 C. At 3 days post injury, animals were imaged and scored for blastema size. Controls were pre-exposed to an equal amount of DMSO, then placed in worm water after amputation. Experiments were run at least 1 time. Total biological replicates: DMSO controls, n = 18; DPI, n = 8; DPI + H_2O_2, n = 10. For Figures 6D–F: 400 μM H_2O_2 was added after amputation concurrent with 200 μT WMF exposure. Experiments were run twice. Total biological replicates: 45 μT, n = 35; 200 μT, n = 28; 200 μT + H_2O_2, n = 23. For Figures 6G–I, animals were presoaked in 400 μM H_2O_2 (Exogenous H_2O_2) or worm water (Untreated Controls) for 24 h prior to amputation and then returned to H_2O_2 (or worm water for controls) for 1 h, at which time all animals were rinsed 3X in worm water and placed in the O_2^- dye orange 1 (as described above) for an additional hour prior to imaging at 2 h post amputation. Experiments were run once. Total biological replicates: H_2O_2, n = 10; untreated, n = 12.

Image collection

A Zeiss V20 Fluorescence Stereomicroscope with an AxioCam MRc or MRm camera and ZEN (lite) software was used for image collection. All live images were taken while regenerates were moving (fully extended) to prevent skewing blastema size/signal intensity due to scrunching. For blastema size, animals were imaged in 100 mm Petri dishes with worm water. For live dyes, animals were imaged in 35 mm FluoroDishes (WPI FD35-100) with 25 mm round no. 1.5 coverslips (WPI 503508). For the general ROS dye CM-H_2DCFDA, heat maps were generated using the standard rainbow lookup table (LUT) to visualize signal intensity. For each assay, samples were imaged at the same magnification and exposure levels to prevent confounding variables during comparisons (*i.e.,* acquisition conditions were kept constant across an experiment between control/treated and/or all different time points). Photoshop (Adobe) was used to orient and scale images (and improve clarity for morphology only). No data was added or subtracted. Original images available by request.

Quantification and statistical analyses

The magnetic lasso tool in Photoshop (Adobe) was used to generate total pixel counts of the anterior blastema (white tissues) and total regenerate (entire worm including blastema). To account for any variation in worm size, blastema was calculated as percent of total body size: (blastema size/body size) x 100. The magnetic lasso tool was also used to measure gray mean values (signal intensity) of fluorescent dyes at the anterior blastema. To account for any variation in dye loading, signal intensity was calculated as the difference between signal at the blastema *versus* signal from the middle of the regenerate (the pharyngeal region): blastema – pharyngeal region. Cell counts of pH3+ were done using the RTNC plugin tool with ImageJ. Number of mitotic cells was expressed as cells per mm^2 of the entire regenerate, with total area measured using the magnetic lasso tool (as before). Significance: either two-tailed Student's t-test with unequal variance (Microsoft Excel or GraphPad Prism 9); or one-way analysis of variance (ANOVA) with Tukey's multiple comparison test (GraphPad Prism 7).

Data availability statement

The original contributions presented in the study are included in the article/Supplementary Material, further inquiries can be directed to the corresponding author.

Author contributions

LK, AV, and WB contributed to conception and design of the study. LK performed the experiments and statistical analyses, with the exception of the *in situ* hybridization experiments and analyses (which were performed by AV). LK wrote the first draft of manuscript. LK and WB contributed to manuscript revision and figure preparation. All authors read and approved the submitted version.

Funding

Funding was provided by grants to WB from the National Science Foundation (EAGER 1644384 and CAREER 1652312) and Western Michigan University (Presidential Innovation Professorship).

Acknowledgments

We would like to gratefully thank Frank Barnes, University of Colorado-Boulder, for the gift and continued use of the MagShield box, along with many invaluable discussions and suggestions over the past years. We additionally thank Christoph Simon and his lab at the University of Calgary for useful conversations, as well as Beane lab members Saad Qureshi for assistance with DPI experiments and Samantha J. Hack for data discussions. Thanks for support also goes to LK. AV was affiliated with Western Michigan University at the time of the study

and is currently affiliated with St. Jude Children's Research Hospital.

Conflict of interest

The authors declare that the research was conducted in the absence of any commercial or financial relationships that could be construed as a potential conflict of interest.

Publisher's note

References

1. Sinenko SA, Starkova TY, Kuzmin AA, Tomilin AN. Physiological signaling functions of reactive oxygen species in stem cells: From flies to man. *Front Cel Dev Biol* (2021) 9:714370. Epub 2021/08/24. doi:10.3389/fcell.2021.714370

2. Jena NR. DNA damage by reactive species: Mechanisms, mutation and repair. *J Biosci* (2012) 37(3):503–17. Epub 2012/07/04. doi:10.1007/s12038-012-9218-2

3. Sies H, Jones DP. Reactive oxygen species (ros) as pleiotropic physiological signalling agents. *Nat Rev Mol Cel Biol* (2020) 21(7):363–83. Epub 2020/04/02. doi:10.1038/s41580-020-0230-3

4. Sreedhar A, Aguilera-Aguirre L, Singh KK. Mitochondria in skin health, aging, and disease. *Cell Death Dis* (2020) 11(6):444. Epub 20200609. doi:10.1038/s41419-020-2649-z

5. Liang J, Wu M, Chen C, Mai M, Huang J, Zhu P. Roles of reactive oxygen species in cardiac differentiation, reprogramming, and regenerative therapies. *Oxid Med Cel Longev* (2020) 2020:2102841–14. Epub 2020/09/11. doi:10.1155/2020/2102841

6. Thauvin M, Matias de Sousa R, Alves M, Volovitch M, Vriz S, Rampon C. An early shh-H2o2 reciprocal regulatory interaction controls the regenerative program during zebrafish fin regeneration. *J Cel Sci* (2022) 135(6):jcs259664. Epub 2022/02/03. doi:10.1242/jcs.259664

7. Tamborindeguy MT, Matte BF, Ramos GO, Alves AM, Bernardi L, Lamers ML. Nadph-oxidase-derived ros alters cell migration by modulating adhesions dynamics. *Biol Cel* (2018) 110(10):225–36. Epub 20180916. doi:10.1111/boc.201800011

8. Diwanji N, Bergmann A. An unexpected friend - ros in apoptosis-induced compensatory proliferation: Implications for regeneration and cancer. *Semin Cel Dev Biol* (2018) 80:74–82. Epub 20170705. doi:10.1016/j.semcdb.2017.07.004

9. Luo Z, Xu X, Sho T, Zhang J, Xu W, Yao J, et al. Ros-induced autophagy regulates porcine trophectoderm cell apoptosis, proliferation, and differentiation. *Am J Physiol Cel Physiol* (2019) 316(2):C198–c209. Epub 20181128. doi:10.1152/ajpcell.00256.2018

10. Bigarella CL, Liang R, Ghaffari S. Stem cells and the impact of ros signaling. *Development* (2014) 141(22):4206–18. Epub 2014/11/06. doi:10.1242/dev.107086

11. Love NR, Chen Y, Ishibashi S, Kritsiligkou P, Lea R, Koh Y, et al. Amputation-induced reactive oxygen species are required for successful Xenopus tadpole tail regeneration. *Nat Cel Biol* (2013) 15(2):222–8. Epub 20130113. doi:10.1038/ncb2659

12. Santabarbara-Ruiz P, Esteban-Collado J, Perez L, Viola G, Abril JF, Milan M, et al. Ask1 and akt act synergistically to promote ros-dependent regeneration in Drosophila. *PLoS Genet* (2019) 15(1):e1007926. Epub 2019/01/25. doi:10.1371/journal.pgen.1007926

13. Gauron C, Rampon C, Bouzaffour M, Ipendey E, Teillon J, Volovitch M, et al. Sustained production of ros triggers compensatory proliferation and is required for regeneration to proceed. *Sci Rep* (2013) 3:2084. Epub 2013/06/28. doi:10.1038/srep02084

14. Al Haj Baddar NW, Chithrala A, Voss SR. Amputation-induced reactive oxygen species signaling is required for axolotl tail regeneration. *Dev Dyn* (2019) 248(2):189–96. Epub 2018/12/21. doi:10.1002/dvdy.5

15. Van Huizen AV, Morton JM, Kinsey LJ, Von Kannon DG, Saad MA, Birkholz TR, et al. Weak magnetic fields alter stem cell-mediated growth. *Sci Adv* (2019) 5(1):eaau7201. Epub 2019/02/08. doi:10.1126/sciadv.aau7201

16. Carrasco E, Calvo MI, Blázquez-Castro A, Vecchio D, Zamarrón A, de Almeida IJD, et al. Photoactivation of ros production *in situ* transiently activates cell proliferation in mouse skin and in the hair follicle stem cell niche promoting hair growth and wound healing. *J Invest Dermatol* (2015) 135(11):2611–22. Epub 2015/07/03. doi:10.1038/jid.2015.248

17. Wei H, Cong X. The effect of reactive oxygen species on cardiomyocyte differentiation of pluripotent stem cells. *Free Radic Res* (2018) 52(2):150–8. Epub 2017/12/21. doi:10.1080/10715762.2017.1420184

18. Tan DQ, Suda T. Reactive oxygen species and mitochondrial homeostasis as regulators of stem cell fate and function. *Antioxid Redox Signal* (2018) 29(2):149–68. Epub 20171026. doi:10.1089/ars.2017.7273

19. Yang S, Lian G. Ros and diseases: Role in metabolism and energy supply. *Mol Cel Biochem* (2020) 467(1-2):1–12. Epub 2019/12/10. doi:10.1007/s11010-019-03667-9

20. Kirtonia A, Sethi G, Garg M. The multifaceted role of reactive oxygen species in tumorigenesis. *Cell Mol Life Sci* (2020) 77(22):4459–83. Epub 2020/05/03. doi:10.1007/s00018-020-03536-5

21. Durand N, Storz P. Targeting reactive oxygen species in development and progression of pancreatic cancer. *Expert Rev Anticancer Ther* (2017) 17(1):19–31. Epub 2016/11/15. doi:10.1080/14737140.2017.1261017

22. Tauffenberger A, Magistretti PJ. Reactive oxygen species: Beyond their reactive behavior. *Neurochem Res* (2021) 46(1):77–87. Epub 2021/01/14. doi:10.1007/s11064-020-03208-7

23. Glass SB, Gonzalez-Fajardo L, Beringhs AO, Lu X. Redox potential and ros-mediated nanomedicines for improving cancer therapy. *Antioxid Redox Signal* (2019) 30(5):747–61. Epub 20171121. doi:10.1089/ars.2017.7370

24. Mitchell MJ, Billingsley MM, Haley RM, Wechsler ME, Peppas NA, Langer R. Engineering precision nanoparticles for drug delivery. *Nat Rev Drug Discov* (2021) 20(2):101–24. Epub 20201204. doi:10.1038/s41573-020-0090-8

25. Brocklehurst B, McLauchlan KA. Free radical mechanism for the effects of environmental electromagnetic fields on biological systems. *Int J Radiat Biol* (1996) 69(1):3–24. Epub 1996/01/01. doi:10.1080/095530096146147

26. Wang K, Ritz T. Zeeman resonances for radical-pair reactions in weak static magnetic fields. *Mol Phys* (2006) 104(10-11):1649–58. doi:10.1080/00268970600564869

27. Barnes FS, Greenebaum B. The effects of weak magnetic fields on radical pairs. *Bioelectromagnetics* (2015) 36(1):45–54. Epub 2014/11/18. doi:10.1002/bem.21883

28. Barnes F, Greenebaum B. Role of radical pairs and feedback in weak radio frequency field effects on biological systems. *Environ Res* (2018) 163:165–70. Epub 2018/02/14. doi:10.1016/j.envres.2018.01.038

29. Barnes F, Greenebaum B. Setting guidelines for electromagnetic exposures and research needs. *Bioelectromagnetics* (2020) 41(5):392–7. Epub 2020/04/21. doi:10.1002/bem.22267

30. Rishabh R, Zadeh-Haghighi H, Salahub D, Simon C. Radical pairs may explain reactive oxygen species-mediated effects of hypomagnetic field on neurogenesis. *Plos Comput Biol* (2022) 18(6):e1010198. Epub 20220602. doi:10.1371/journal.pcbi.1010198

31. Buemi M, Marino D, Di Pasquale G, Floccari F, Senatore M, Aloisi C, et al. Cell proliferation/cell death balance in renal cell cultures after exposure to a static magnetic field. *Nephron* (2001) 87(3):269–73. Epub 2001/04/05. doi:10.1159/000045925

32. Bekhite MM, Finkensieper A, Abou-Zaid FA, El-Shourbagy IK, Omar KM, Figulla HR, et al. Static electromagnetic fields induce vasculogenesis and chondro-osteogenesis of mouse embryonic stem cells by reactive oxygen species-mediated up-regulation of vascular endothelial growth factor. *Stem Cell Dev* (2010) 19(5):731–43. Epub 2009/10/01. doi:10.1089/scd.2008.0266

33. Fu JP, Mo WC, Liu Y, He RQ. Decline of cell viability and mitochondrial activity in mouse skeletal muscle cell in a hypomagnetic field. *Bioelectromagnetics* (2016) 37(4):212–22. Epub 2016/03/24. doi:10.1002/bem.21968

34. Martino CF, Castello PR. Modulation of hydrogen peroxide production in cellular systems by low level magnetic fields. *PLoS One* (2011) 6(8):e22753. Epub 2011/09/03. doi:10.1371/journal.pone.0022753

35. Ermakov A, Afanasyeva V, Ermakova O, Blagodatski A, Popov A. Effect of weak alternating magnetic fields on planarian regeneration. *Biochem Biophys Res Commun* (2022) 592:7–12. Epub 20211228. doi:10.1016/j.bbrc.2021.12.096

36. Baguna J, Salo E, Auladell C. Regeneration and pattern formation in planarians. III. that neoblasts are totipotent stem cells and the cells. *Development* (1989) 107:77–86. doi:10.1242/dev.107.1.77

37. Wenemoser D, Lapan SW, Wilkinson AW, Bell GW, Reddien PW. A molecular wound response program associated with regeneration initiation in planarians. *Genes Dev* (2012) 26(9):988–1002. Epub 2012/05/03. doi:10.1101/gad.187377.112

38. Eisenhoffer GT, Kang H, Sanchez Alvarado A. Molecular analysis of stem cells and their descendants during cell turnover and regeneration in the planarian Schmidtea mediterranea. *Cell stem cell* (2008) 3(3):327–39. doi:10.1016/j.stem.2008.07.002

39. Pirotte N, Stevens AS, Fraguas S, Plusquin M, Van Roten A, Van Belleghem F, et al. Reactive oxygen species in planarian regeneration: An upstream necessity for correct patterning and brain formation. *Oxid Med Cel Longev* (2015) 2015:1–19. Epub 2015/07/17. doi:10.1155/2015/392476

40. Jaenen V, Fraguas S, Bijnens K, Heleven M, Artois T, Romero R, et al. Reactive oxygen species rescue regeneration after silencing the mapk-erk signaling pathway in Schmidtea mediterranea. *Scientific Rep* (2021) 11(1):881. Epub 2021/01/15. doi:10.1038/s41598-020-79588-1

41. Birkholz TR, Van Huizen AV, Beane WS. Staying in shape: Planarians as a model for understanding regenerative morphology. *Semin Cel Dev Biol* (2018) 87:105–15. Epub 2018/05/09. doi:10.1016/j.semcdb.2018.04.014

42. Matokanovic M, Barisic K, Filipovic-Grcic J, Maysinger D. Hsp70 silencing with sirna in nanocarriers enhances cancer cell death induced by the inhibitor of Hsp90. *Eur J Pharm Sci* (2013) 50(1):149–58. Epub 2013/04/16. doi:10.1016/j.ejps.2013.04.001

43. Shende P, Bhandarkar S, Prabhakar B. Heat shock proteins and their protective roles in stem cell biology. *Stem Cel Rev Rep* (2019) 15(5):637–51. Epub 2019/06/30. doi:10.1007/s12015-019-09903-5

44. Isolani ME, Conte M, Deri P, Batistoni R. Stem cell protection mechanisms in planarians: The role of some heat shock genes. *Int J Dev Biol* (2012) 56(1-3):127–33. Epub 2012/03/28. doi:10.1387/ijdb.113432mi

45. Sies H. Hydrogen peroxide as a central redox signaling molecule in physiological oxidative stress: Oxidative eustress. *Redox Biol* (2017) 11:613–9. Epub 20170105. doi:10.1016/j.redox.2016.12.035

46. Buetler TM, Krauskopf A, Ruegg UT. Role of superoxide as a signaling molecule. *News Physiol Sci* (2004) 19:120–3. doi:10.1152/nips.01514.2003

47. Bijnens K, Jaenen V, Wouters A, Leynen N, Pirotte N, Artois T, et al. A spatiotemporal characterisation of redox molecules in planarians, with a focus on the role of glutathione during regeneration. *Biomolecules* (2021) 11(5):714. Epub 20210511. doi:10.3390/biom11050714

48. Reis J, Massari M, Marchese S, Ceccon M, Aalbers FS, Corana F, et al. A closer look into nadph oxidase inhibitors: Validation and insight into their mechanism of action. *Redox Biol* (2020) 32:101466. Epub 20200215. doi:10.1016/j.redox.2020.101466

49. Altenhofer S, Radermacher KA, Kleikers PW, Wingler K, Schmidt HH. Evolution of nadph oxidase inhibitors: Selectivity and mechanisms for target engagement. *Antioxid Redox Signal* (2015) 23(5):406–27. Epub 20140226. doi:10.1089/ars.2013.5814

50. Liaudet L, Vassalli G, Pacher P. Role of peroxynitrite in the redox regulation of cell signal transduction pathways. *Front Biosci (Landmark Ed* (2009) 14(12):4809–14. Epub 20090101. doi:10.2741/3569

51. Piacenza L, Zeida A, Trujillo M, Radi R. The superoxide radical switch in the biology of nitric oxide and peroxynitrite. *Physiol Rev* (2022) 102(4):1881–906. Epub 20220523. doi:10.1152/physrev.00005.2022

52. Zhang J, Ding C, Ren L, Zhou Y, Shang P. The effects of static magnetic fields on bone. *Prog Biophys Mol Biol* (2014) 114(3):146–52. Epub 2014/02/22. doi:10.1016/j.pbiomolbio.2014.02.001

53. Okano H. Effects of static magnetic fields in biology: Role of free radicals. *Front Biosci* (2008) 13:6106–25. Epub 2008/05/30. doi:10.2741/3141

54. Caballano-Infantes E, Cahuana GM, Bedoya FJ, Salguero-Aranda C, Tejedo JR. The role of nitric oxide in stem cell biology. *Antioxidants (Basel)* (2022) 11(3):497. Epub 20220303. doi:10.3390/antiox11030497

55. Zadeh-Haghighi H, Simon C. Magnetic field effects in biology from the perspective of the radical pair mechanism. *J R Soc Interf* (2022) 19(193):20220325. doi:10.1098/rsif.2022.0325

56. Gurhan H, Bruzon R, Kandala S, Greenebaum B, Barnes F. Effects induced by a weak static magnetic field of different intensities on ht-1080 fibrosarcoma cells. *Bioelectromagnetics* (2021) 42(3):212–23. Epub 2021/03/19. doi:10.1002/bem.22332

57. Holmström KM, Finkel T. Cellular mechanisms and physiological consequences of redox-dependent signalling. *Nat Rev Mol Cel Biol* (2014) 15(6):411–21. Epub 2014/05/24. doi:10.1038/nrm3801

58. Adams L, Franco MC, Estevez AG. Reactive nitrogen species in cellular signaling. *Exp Biol Med (Maywood)* (2015) 240(6):711–7. Epub 20150416. doi:10.1177/1535370215581314

59. Xiao Y, Li X, Cui Y, Zhang J, Liu L, Xie X, et al. Hydrogen peroxide inhibits proliferation and endothelial differentiation of bone marrow stem cells partially via reactive oxygen species generation. *Life Sci* (2014) 112(1-2):33–40. Epub 20140721. doi:10.1016/j.lfs.2014.07.016

60. Chu L, Jiang Y, Hao H, Xia Y, Xu J, Liu Z, et al. Nitric oxide enhances oct-4 expression in bone marrow stem cells and promotes endothelial differentiation. *Eur J Pharmacol* (2008) 591(1-3):59–65. Epub 20080622. doi:10.1016/j.ejphar.2008.06.066

61. Carbonell MB, Zapata Cardona J, Delgado JP. Hydrogen peroxide is necessary during tail regeneration in juvenile axolotl. *Dev Dyn* (2022) 251(6):1054–76. Epub 20210624. doi:10.1002/dvdy.386

62. LeBert D, Squirrell JM, Freisinger C, Rindy J, Golenberg N, Frecentese G, et al. Damage-induced reactive oxygen species regulate vimentin and dynamic collagen-based projections to mediate wound repair. *Elife* (2018) 7:e30703. Epub 20180116. doi:10.7554/eLife.30703

63. Han P, Zhou XH, Chang N, Xiao CL, Yan S, Ren H, et al. Hydrogen peroxide primes heart regeneration with a derepression mechanism. *Cell Res* (2014) 24(9):1091–107. Epub 2014/08/16. doi:10.1038/cr.2014.108

64. Radi R. Oxygen radicals, nitric oxide, and peroxynitrite: Redox pathways in molecular medicine. *Proc Natl Acad Sci United States America* (2018) 115(23):5839–48. Epub 20180525. doi:10.1073/pnas.1804932115

65. Speckmann B, Steinbrenner H, Grune T, Klotz LO. Peroxynitrite: From interception to signaling. *Arch Biochem Biophys* (2016) 595:153–60. doi:10.1016/j.abb.2015.06.022

66. Policar C, Bouvet J, Bertrand HC, Delsuc N. Sod mimics: From the tool box of the chemists to cellular studies. *Curr Opin Chem Biol* (2022) 67:102109. Epub 20220120. doi:10.1016/j.cbpa.2021.102109

67. Alvarez B, Radi R. Peroxynitrite reactivity with amino acids and proteins. *Amino Acids* (2003) 25(3-4):295–311. Epub 20030926. doi:10.1007/s00726-003-0018-8

68. Ferrer-Sueta G, Radi R. Chemical biology of peroxynitrite: Kinetics, diffusion, and radicals. *ACS Chem Biol* (2009) 4(3):161–77. doi:10.1021/cb800279q

69. Chen X, Zhou B, Yan T, Wu H, Feng J, Chen H, et al. Peroxynitrite enhances self-renewal, proliferation and neuronal differentiation of neural stem/progenitor cells through activating hif-1α and wnt/B-catenin signaling pathway. *Free Radic Biol Med* (2018) 117:158–67. Epub 20180207. doi:10.1016/j.freeradbiomed.2018.02.011

70. Gladyshev VN. The free radical theory of aging is dead. Long live the damage theory. *Antioxid Redox Signal* (2014) 20(4):727–31. Epub 20131204. doi:10.1089/ars.2013.5228

71. Demicheli V, Moreno DM, Radi R. Human Mn-superoxide dismutase inactivation by peroxynitrite: A paradigm of metal-catalyzed tyrosine nitration *in vitro* and *in vivo*. *Metallomics* (2018) 10(5):679–95. doi:10.1039/c7mt00348j

72. Abnave P, Aboukhatwa E, Kosaka N, Thompson J, Hill MA, Aboobaker AA (2017). Epithelial-mesenchymal transition transcription factors control pluripotent adult stem cell migration *in vivo* in planarians, *Development* 144, 3440–53. Epub 20170911. doi:10.1242/dev.154971

73. Sahu S, Sridhar D, Abnave P, Kosaka N, Dattani A, Thompson JM, et al. Ongoing repair of migration-coupled DNA damage allows planarian adult stem cells to reach wound sites. *eLife* (2021) 10:e63779. Epub 20210423. doi:10.7554/eLife.63779

74. Sadok A, Bourgarel-Rey V, Gattacceca F, Penel C, Lehmann M, Kovacic H. Nox1-Dependent superoxide production controls colon adenocarcinoma cell migration. *Biochim Biophys Acta* (2008) 1783(1):23–33. Epub 20071030. doi:10.1016/j.bbamcr.2007.10.010

75. Miles RR, Amin PH, Diaz MB, Misra J, Aukerman E, Das A, et al. The Eif2 kinase Gcn2 directs keratinocyte collective cell migration during wound healing via coordination of reactive oxygen species and amino acids. *J Biol Chem* (2021) 297(5):101257. Epub 20210929. doi:10.1016/j.jbc.2021.101257

76. Chen YH, Hsu JY, Chu CT, Chang YW, Fan JR, Yang MH, et al. Loss of cell-cell adhesion triggers cell migration through rac1-dependent ros generation. *Life Sci Alliance* (2023) 6(2):e202201529. Epub 20221129. doi:10.26508/lsa.202201529

77. Boudreau HE, Leto TL. Model systems to investigate nox-dependent cell migration and invasiveness. *Methods Mol Biol* (2019) 1982:473–85. doi:10.1007/978-1-4939-9424-3_28

78. Li Y, Liang R, Zhang X, Wang J, Shan C, Liu S, et al. Copper chaperone for superoxide dismutase promotes breast cancer cell proliferation and migration via ros-mediated mapk/erk signaling. *Front Pharmacol* (2019) 10:356. Epub 20190405. doi:10.3389/fphar.2019.00356

79. Mesquita APS, Matsuoka M, Lopes SA, Pernambuco Filho PCA, Cruz AS, Nader HB, et al. Nitric oxide regulates adhesiveness, invasiveness, and migration of anoikis-resistant endothelial cells. *Braz J Med Biol Res* (2022) 55:e11612. Epub 20220204. doi:10.1590/1414-431X2021e11612

80. Tejero J, Shiva S, Gladwin MT. Sources of vascular nitric oxide and reactive oxygen species and their regulation. *Physiol Rev* (2019) 99(1):311–79. doi:10.1152/physrev.00036.2017

81. Kandhwal M, Behl T, Kumar A, Arora S. Understanding the potential role and delivery approaches of nitric oxide in chronic wound healing management. *Curr Pharm Des* (2021) 27(17):1999–2014. doi:10.2174/1381612826666201026152209

82. Okamura DM, Nguyen ED, Beier DR, Majesky MW. Wound healing and regeneration in spiny mice (Acomys cahirinus). *Curr Top Dev Biol* (2022) 148:139–64. Epub 20220325. doi:10.1016/bs.ctdb.2022.03.001

83. Zahid AA, Ahmed R, Ur Rehman SR, Augustine R, Hasan A. Reactive nitrogen species releasing hydrogel for enhanced wound healing. *Annu Int Conf IEEE Eng Med Biol Soc* (2019) 2019:3939–42. doi:10.1109/embc.2019.8856469

84. Tavares G, Alves P, Simoes P. Recent advances in hydrogel-mediated nitric oxide delivery systems targeted for wound healing applications. *Pharmaceutics* (2022) 14(7):1377. Epub 20220629. doi:10.3390/pharmaceutics14071377

85. Zhan R, Wang F, Wu Y, Wang Y, Qian W, Liu M, et al. Nitric oxide promotes epidermal stem cell proliferation via Foxg1-C-myc signalling. *Nitric Oxide* (2018) 73:1–8. Epub 20171214. doi:10.1016/j.niox.2017.12.002

86. Szeliga M, Albrecht J. Roles of nitric oxide and polyamines in brain tumor growth. *Adv Med Sci* (2021) 66(1):199–205. Epub 20210309. doi:10.1016/j.advms.2021.02.006

87. Matrone G, Jung SY, Choi JM, Jain A, Leung HE, Rajapakshe K, et al. Nuclear S-nitrosylation impacts tissue regeneration in zebrafish. *Nat Commun* (2021) 12(1):6282. Epub 20211101. doi:10.1038/s41467-021-26621-0

88. Wang L, Kuang Z, Zhang D, Gao Y, Ying M, Wang T. Reactive oxygen species in immune cells: A new antitumor target. *Biomed Pharmacother* (2021) 133:110978. Epub 2020/11/12. doi:10.1016/j.biopha.2020.110978

89. Sorolla MA, Hidalgo I, Sorolla A, Montal R, Pallisé O, Salud A, et al. Microenvironmental reactive oxygen species in colorectal cancer: Involved processes and therapeutic opportunities. *Cancers (Basel)* (2021) 13(20):5037. Epub 20211009. doi:10.3390/cancers13205037

90. Nguyen GT, Green ER, Mecsas J. Neutrophils to the roscue: Mechanisms of nadph oxidase activation and bacterial resistance. *Front Cell Infect Microbiol* (2017) 7:373. Epub 20170825. doi:10.3389/fcimb.2017.00373

91. Tavassolifar MJ, Vodjgani M, Salehi Z, Izad M. The influence of reactive oxygen species in the immune system and pathogenesis of multiple sclerosis. *Autoimmune Dis* (2020) 2020:1–14. Epub 20200625. doi:10.1155/2020/5793817

92. Beane WS, Morokuma J, Lemire JM, Levin M. Bioelectric signaling regulates head and organ size during planarian regeneration. *Development* (2013) 140(2):313–22. Epub 2012/12/20. doi:10.1242/dev.086900

93. Pearson BJ, Eisenhoffer GT, Gurley KA, Rink JC, Miller DE, Sanchez Alvarado A. Formaldehyde-based whole-mount *in situ* hybridization method for planarians. *Dev Dyn* (2009) 238(2):443–50. doi:10.1002/dvdy.21849

94. Beane WS, Tseng AS, Morokuma J, Lemire JM, Levin M. Inhibition of planar cell polarity extends neural growth during regeneration, homeostasis, and development. *Stem Cell Dev* (2012) 21(12):2085–94. Epub 2012/02/22. doi:10.1089/scd.2011.0605